

RESEARCH OUTPUTS / RÉSULTATS DE RECHERCHE

The Greatwall-Endosulfine-PP2A/B55 pathway regulates entry into quiescence by enhancing translation of Elongator-tunable transcripts

Encinar del Dedo, Javier; Suárez, M. Belén; López-San Segundo, Rafael; Vázquez-Bolado, Alicia; Sun, Jingjing; García-Blanco, Natalia; García, Patricia; Tricquet, Pauline; Chen, Jun Song; Dedon, Peter C.; Gould, Kathleen L.; Hidalgo, Elena; Hermand, Damien; Moreno, Sergio

Published in:
Nature Communications

DOI:
[10.1038/s41467-024-55004-4](https://doi.org/10.1038/s41467-024-55004-4)

Publication date:
2024

Document Version
Publisher's PDF, also known as Version of record

[Link to publication](#)

Citation for published version (HARVARD):

Encinar del Dedo, J, Suárez, MB, López-San Segundo, R, Vázquez-Bolado, A, Sun, J, García-Blanco, N, García, P, Tricquet, P, Chen, JS, Dedon, PC, Gould, KL, Hidalgo, E, Hermand, D & Moreno, S 2024, 'The Greatwall-Endosulfine-PP2A/B55 pathway regulates entry into quiescence by enhancing translation of Elongator-tunable transcripts', *Nature Communications*, vol. 15, no. 1, 10603. <https://doi.org/10.1038/s41467-024-55004-4>

General rights

Copyright and moral rights for the publications made accessible in the public portal are retained by the authors and/or other copyright owners and it is a condition of accessing publications that users recognise and abide by the legal requirements associated with these rights.

- Users may download and print one copy of any publication from the public portal for the purpose of private study or research.
- You may not further distribute the material or use it for any profit-making activity or commercial gain
- You may freely distribute the URL identifying the publication in the public portal ?

Take down policy

If you believe that this document breaches copyright please contact us providing details, and we will remove access to the work immediately and investigate your claim.



The Greatwall-Endosulfine-PP2A/B55 pathway regulates entry into quiescence by enhancing translation of Elongator-tunable transcripts

Received: 15 November 2023

Accepted: 27 November 2024

Published online: 05 December 2024

 Check for updates

Javier Encinar del Dedo¹  , M. Belén Suárez^{2,3,10}, Rafael López-San Segundo^{1,10}, Alicia Vázquez-Bolado^{1,10}, Jingjing Sun⁴, Natalia García-Blanco¹, Patricia García^{1,2,3} , Pauline Tricquet^{1,5} , Jun-Song Chen⁶, Peter C. Dedon^{1,4,7} , Kathleen L. Gould^{1,6} , Elena Hidalgo^{1,8} , Damien Hermand^{1,5,9}  & Sergio Moreno¹  

Quiescent cells require a continuous supply of proteins to maintain protein homeostasis. In fission yeast, entry into quiescence is triggered by nitrogen stress, leading to the inactivation of TORC1 and the activation of TORC2. In this study, we demonstrate that the Greatwall-Endosulfine-PPA/B55 pathway connects the downregulation of TORC1 with the upregulation of TORC2, resulting in the activation of Elongator-dependent tRNA modifications crucial for sustaining the translation programme during entry into quiescence. This mechanism promotes U₃₄ and A₃₇ tRNA modifications at the anticodon stem loop, enhancing translation efficiency and fidelity of mRNAs enriched for AAA versus AAG lysine codons. Notably, several of these mRNAs encode TORC1 inhibitors, TORC2 activators, tRNA modifiers, and proteins necessary for telomeric and subtelomeric functions. Therefore, we propose a mechanism by which cells respond to nitrogen stress at the level of translation, involving a coordinated interplay between tRNA epitranscriptome and biased codon usage.

Most cells in living organisms rest in a non-dividing state called the G0 phase, also known as quiescence. Quiescent cells can re-enter the cell cycle with full viability when provided with the appropriate signals. Examples of quiescent cells include stem cells, neuronal progenitor cells, memory T cells, eggs, and spores. Despite their importance, the

molecular mechanisms governing quiescence entry, its maintenance, and exit are not yet fully understood.

In nature, unicellular organisms continuously enter and exit quiescence depending on nutrient availability. In fission yeast, entry into quiescence is induced by nitrogen starvation, resulting in the

¹Instituto de Biología Funcional y Genómica, CSIC, University of Salamanca, 37007 Salamanca, Spain. ²Instituto de Biología Funcional y Genómica, University of Salamanca, CSIC, 37007 Salamanca, Spain. ³Departamento de Microbiología y Genética, University of Salamanca, 37007 Salamanca, Spain. ⁴Antimicrobial Resistance Interdisciplinary Research Group, Singapore-MIT Alliance for Research and Technology, Singapore, Singapore. ⁵URPHYM-GEMO, University of Namur, rue de Bruxelles, 61, Namur 5000, Belgium. ⁶Department of Cell and Developmental Biology, Vanderbilt University School of Medicine, Nashville, TN, USA. ⁷Department of Biological Engineering and Center for Environmental Health Science, Massachusetts Institute of Technology, Cambridge, MA, USA. ⁸Oxidative Stress and Cell Cycle Group, Universitat Pompeu Fabra, 08003 Barcelona, Spain. ⁹The Francis Crick Institute, 1 Midland Road London, London NW1 1AT, UK. ¹⁰These authors contributed equally: M. Belén Suárez, Rafael López-San Segundo, Alicia Vázquez-Bolado. ✉ e-mail: jedel_dedo@usal.es; smo@usal.es

inactivation of TOR complex 1 (TORC1) and the activation of TOR complex 2 (TORC2). TORC1 promotes cell growth in response to nutrients, growth factors, or cellular energy^{1,2}, while TORC2 is required for the nutrient stress response, cell survival during quiescence, and cell differentiation^{3–5}. The activation of the Greatwall-Endosulfine switch upon TORC1 inactivation leads to inhibition of the PP2A/B55 protein phosphatase, which is necessary for switching on TORC2 activity by increasing Gad8 phosphorylation^{4–7}.

TORC2 activation also regulates protein translation by controlling tRNA modifications through the Elongator complex⁸. Elongator is a multiprotein complex that modifies the anticodon stem loop of tRNA^{Lys}_{UUU}, tRNA^{Glu}_{UUC} and tRNA^{Gln}_{UUG} by introducing an acetyl group at position 5 of U₃₄ (cm⁵U₃₄), which is further modified by Trm112-Trm9, a methyltransferase complex involved in the formation of mcm⁵U₃₄, and by Ctu1-Ctu2 complex, which catalyses the thiolation at carbon 2 of U₃₄ (mcm⁵s²U₃₄). These U₃₄ modifications counteract codon misreading resulting from low effective stacking interactions between A-U bases^{9–11}. They also play a crucial role in maintaining translational fidelity under stress conditions^{12–15}. Thus, Elongator is necessary for the efficient translation of mRNAs with a high AAA codon usage.

Previous studies have reported a feedback loop between the TORC1-TORC2 signalling cascade and the Elongator complex. In this loop, Elongator plays an essential role in the translation of key components of TORC2 and repressors of TORC1. Additionally, the TORC2 pathway functions as an activator of Elongator by down-regulating Gsk3, a glycogen synthase kinase that inhibits Elongator by phosphorylating the Efp4 subunit at Serine114^{8,16,17}.

In this study, we report that elevated PP2A/B55 phosphatase activity, resulting from the deletion of Endosulfine (*igo1Δ*), impairs the translation efficiency of mRNAs enriched in AAA codons during entry into quiescence. Additionally, we demonstrate a physical and functional interaction between PP2A/B55 and Gad8, Trm112, Ctu1, and the Elongator complex. Furthermore, hyperactivation of PP2A/B55 protein phosphatase reduces the function of the Elongator complex and the amount of Trm112, Ctu1 and Cgi121 proteins, which are essential for U₃₄ and A₃₇ tRNA modifications at the anticodon stem loop. This reduction in translational efficiency leads to decreased protein levels from transcripts containing high AAA codon usage, such as *rap1*, *sgo2*, *lem2*, *clr2*, or *clr3*, all of which are crucial for telomeric and subtelomeric organisation. This induces telomeric detachment, upregulation of subtelomeric gene expression, and eventually, cell death. Our findings suggest that the Greatwall-Endosulfine-PP2A/B55 pathway regulates the translational programme during entry into quiescence by controlling U₃₄ and A₃₇ tRNA modifications. We propose that, in response to nitrogen starvation, cells implement an alternative gene expression programme by translating mRNAs enriched in sub-optimal AAA codons, through the activation of tRNA-modifying complexes.

Results

The Greatwall-Endosulfine switch regulates telomere silencing and telomere attachment to the nuclear envelope

To understand the function of the Greatwall-Endosulfine-PP2A/B55 pathway during entry into quiescence we compared the transcriptome of the wild-type (WT) and the Endosulfine mutant (*igo1Δ*) by RNAseq after shifting cells from nitrogen-rich (EMM2) to nitrogen-free (EMM2-N) media at times 0 and 4 h. In nitrogen-rich medium (EMM2, time 0) the transcriptome was almost identical between the two strains. However, after 4 h of nitrogen starvation, we found significant changes in subtelomeric gene expression, as *igo1Δ* cells showed a high expression level (more than 10-fold) of a group of subtelomeric genes in chromosomes I and II compared to wild-type cells (Fig. 1a; Supplementary Data 1). Most of these genes (95%) remained silenced in wild-type cells after 4 hours of nitrogen starvation. Similar results were obtained when we analysed the

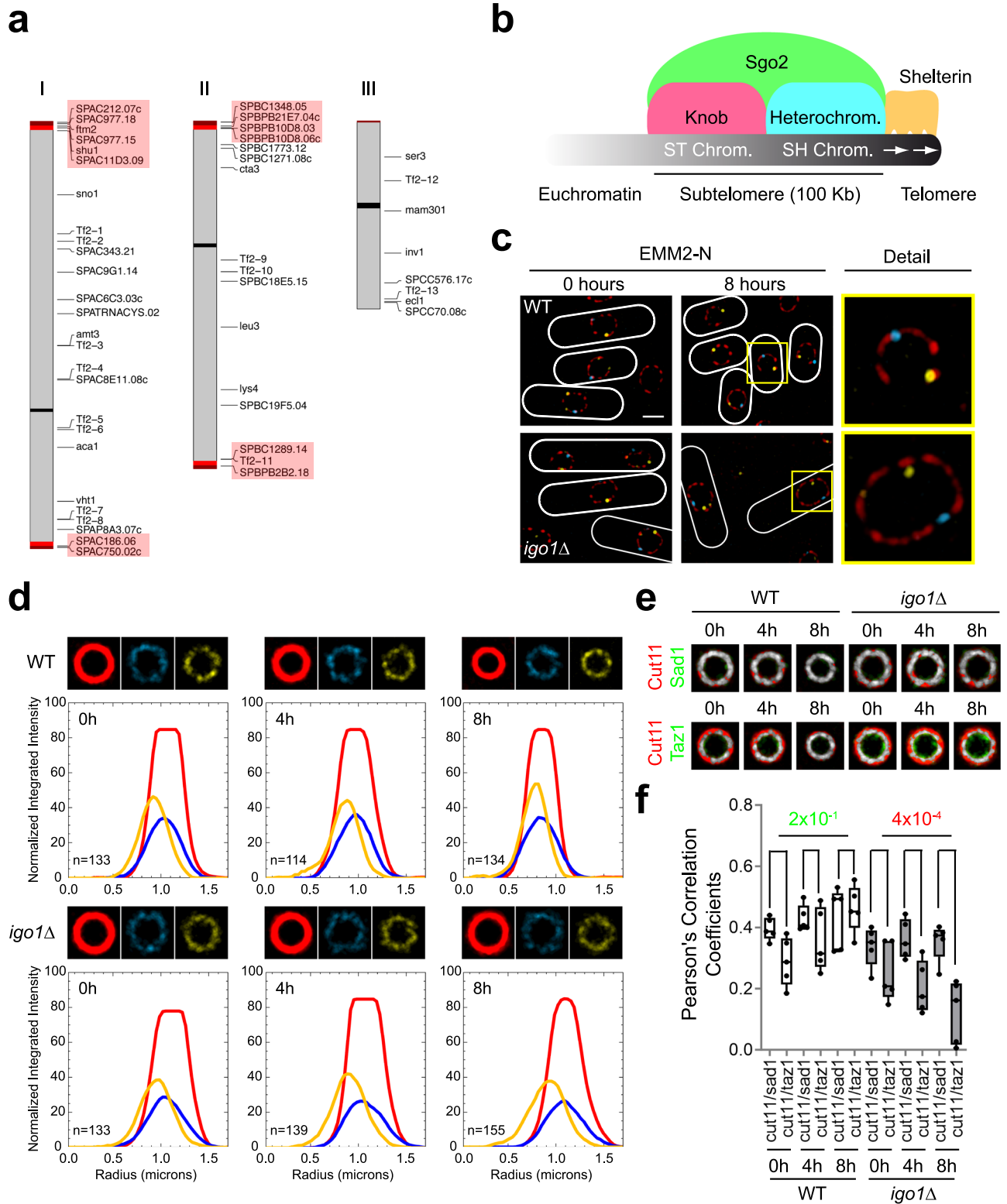
transcriptome of the Greatwall (*ppk18Δ cek1Δ*) mutant (Supplementary Fig. 1a; Supplementary Data 2), consistent with the fact that the Greatwall-Endosulfine-PP2A/B55 is a linear pathway⁴. These results suggest that downregulation of PP2A/B55 plays a key role in transcriptional silencing of subtelomeric genes during quiescence entry.

The ends of chromosomes I and II are composed of telomeric repeats and the subtelomeric regions. While the telomeric repeats extend approximately 300 bp, the subtelomeric regions consist of about 100 kilobases between the telomeric repeats and the euchromatin (Fig. 1b). The heterochromatin present in the subtelomeric regions can be divided into SH chromatin, characterised by highly methylated histone H3K9, and ST chromatin, in which histone modifications are kept at low levels, but exhibit highly condensed chromosome structures called *knobs*^{18–22}. Several protein complexes essential for maintaining the telomeric and subtelomeric structure have been identified. For example, Rap1 (a component of the shelterin complex) and Bqt4 (a component of the bouquet complex) create a molecular link between telomeres and the nuclear envelope^{23–26}. Proteins such as Swi6, the SHREC complex or the CLRC complex play a role in H3K9 methylation, control nucleosome maintenance and genome stability^{27,28}. Finally, shugoshin 2, Sgo2, is an essential protein for condensation of ST chromatin and *knob* stability^{21,22} (Fig. 1b).

To study the role of the Greatwall-Endosulfine-PP2A/B55 pathway in telomeric organisation during quiescence, we analysed nuclear-telomeric attachment in the wild-type (WT) and in the Endosulfine (*igo1Δ*) mutant in nitrogen-rich media (EMM2) and after 8 h of nitrogen starvation (EMM2-N) using Super-Resolution Radial Fluctuations (SRRF) microscopy. Wild-type and *igo1Δ* cells tagged with Cut11-mCherry (a nuclear envelope -NE- marker), Sad1-CFP (a spindle pole body -SPB- marker) and Taz1-YFP (a telomeric marker), showed no significant differences in nitrogen-rich media. In contrast, after 8 h of nitrogen starvation, the *igo1Δ* mutant showed telomeric detachment from the NE (Fig. 1c). To analyse the defect of the *igo1Δ* mutant in more detail, we combined SRRF microscopy with Radial Profile Analysis (see details in Supplementary Fig. 1b and Methods). The wild-type and *igo1Δ* mutant showed a perfect overlap between the NE signal (red line) and the SPB signal (blue line). However, we detected differences in the telomeric signals (yellow line) between strains. While in the wild-type strain the three signals overlapped more with time (4 and 8 h of nitrogen starvation), in the *igo1Δ* mutant, the telomeric signal separated from the NE and the SPB signals (Fig. 1d). A similar result was obtained when we analysed the overlap between the mean NE signal and the mean SPB signal or the mean NE signal and the mean telomeric signal at different time points (Fig. 1e). Statistical analysis allowed us to identify significant differences between Cut11/Sad1 and Cut11/Taz1 signals in the wild-type and the *igo1Δ* mutant (Fig. 1f). These results indicate that the interaction between the NE and telomeres is lost in the *igo1Δ* mutant.

Telomeric detachment is mediated by reduced levels of the Rap1 protein, a component of the shelterin complex

A high level of PP2A/B55 activity, caused by deleting *igo1*, delays entry into mitosis during vegetative growth when fission yeast cells are shifted from a nitrogen-rich to a nitrogen-poor medium, or during entry into quiescence⁴. Therefore, it seemed possible that elevated PP2A/B55 activity caused telomeric detachment during entry into quiescence. In *S. pombe*, two different complexes have been described as essential for maintaining telomeric-NE attachment, the bouquet complex and the shelterin complex. Interestingly, two subunits of the shelterin complex, Rap1 and Ccq1, have been described as heavily phosphorylated proteins^{25,26,29,30}. Thus, we considered that the phosphorylation state of these proteins might be affected by the high PP2A/B55 phosphatase activity in the *igo1Δ* mutant, triggering telomeric detachment. However, we did not detect changes in the phosphorylation state of either Rap1 or Ccq1. Surprisingly, we detected a dramatic reduction in the amount of Rap1 protein levels in the *igo1Δ*



mutant, while the Ccq1 levels remained constant during the experiment (Fig. 2a). To confirm this data and improve our temporal resolution, we repeated the experiment taking samples every 30 min during the first 2 h and then after 4 h of nitrogen starvation. Once more, we detected a very significant decrease in Rap1 protein levels after 2–4 h of nitrogen deprivation in the *igo1Δ* mutant (Fig. 2b, c, left panel).

Previous results from our lab have shown that *igo1Δ* phenotypes could be restored by decreasing PP2A/B55 activity³¹, including the

reduction in viability during quiescence (Supplementary Fig. 2a). This prompted us to investigate whether a reduction of PP2A/B55 activity could restore Rap1 protein levels. To modulate PP2A/B55 activity, we placed the *pab1* open reading frame, encoding the PP2A B55 regulatory subunit, under the control of the thiamine-repressible *nmt41* promoter at its chromosomal locus. We found that repressing Pab1 production and therefore PP2A/B55 activity reinstated Rap1 protein levels (Fig. 2c). Data quantification further confirmed the restoration of Rap1 protein levels when PP2A/B55 activity was reduced (Fig. 2d).

Fig. 1 | The Greatwall-Endosulfine switch regulates subtelomeric gene silencing and telomeric anchoring to the nuclear envelope. **a** Schematic representation of transcriptionally upregulated genes in the Endosulfine (*igo1Δ*) mutant. Genes overexpressed more than 10-fold in *igo1Δ* cells compared to the wild-type after 4 h in nitrogen-free EMM2 medium. Subtelomeric genes are highlighted in red. $n = 3$. **b** Schematic illustration of *S. pombe* subtelomeric chromatin structure (modified from⁸⁶). **c** Representative Super-Resolution Radial Fluctuations (SRRF) micrographs of wild-type (WT) and *igo1Δ* cells expressing Cut11:mCherry, Sad1:CFP and Taz1:YFP in nitrogen-rich EMM2 media (0 h) and after 8 h of nitrogen starvation in EMM2-N. The merged image and a detail view are shown. Bar: 2 μm. **d** Radial Profile Analysis for WT and *igo1Δ* cells after 0, 4 or 8 h of nitrogen deprivation (see details in Supplementary Fig. 1b). The average projection signals for the NE (in red), the SPB (in cyan) and the telomeres (in yellow) are shown. The graphs represent the

normalized integrated intensity as a function of distance in microns. The red lines correspond to the NE signal, the cyan lines correspond to the SPB signal and the yellow lines correspond to the telomeric signal. Over 100 nuclei were analysed at each time point, $n = 3$. **e** Overlay between the average projection signals for Cut11/Sad1 or Cut11/Taz1 in WT and *igo1Δ* cells during entry into quiescence. The images were generated by projecting at least 100 nuclei, $n = 3$. **f** Colocalisation between Cut11/Sad1 and Cut11/Taz1 signals was quantified as Pearson correlation coefficients using ImageJ software. ANCOVA p -values are indicated, with significant differences shown in red. The box extends from the 25th to the 75th percentiles, with the horizontal line indicating the median. The whiskers extend to the minimum and maximum values. $n = 5$ (with at least 20 nuclei analysed per assay). Source data are provided as a Source data file.

To investigate whether reducing PP2A/B55 activity could also prevent telomeric detachment *in vivo*, we examined the localisation of Taz1-YFP in strains exhibiting low PP2A/B55 activity (wild-type and *igo1Δ P_{nut}41:GST:pab1* + Thiamine) in comparison to strains with elevated PP2A/B55 activity (*igo1Δ* and *igo1Δ P_{nut}41:GST:pab1* - Thiamine) during nitrogen starvation. Our analysis showed that low PP2A/B55 activity restored the telomeric detachment phenotype, whereas high PP2A/B55 activity maintained the telomeric attachment defect (Fig. 2e; Supplementary Fig. 2b). Statistical analysis of the data confirmed that reduced PP2A/B55 activity during nitrogen starvation was necessary for preserving telomeric organisation during quiescence (Fig. 2f). Repression of *pab1* expression also rescued the upregulation of subtelomeric genes in nitrogen-starved *igo1Δ* cells (Supplementary Data 3). In summary, these findings suggest that the downregulation of PP2A/B55 activity during entry into quiescence is crucial for maintaining Rap1 protein levels, anchoring telomeres to the NE and silencing the expression of subtelomeric genes.

Sgo2, Clr2 and Clr3 protein levels are reduced in quiescent *igo1Δ* mutant cells

Different protein complexes coordinately maintain chromatin silencing in subtelomeric regions during quiescence in fission yeast. One of the critical factors for this regulation is shugoshin 2, Sgo2. Sgo2 is essential for the formation of *knobs*, highly condensed chromatin structures organised close to the ends of chromosomes I and II²¹. Lack of Sgo2 (*sgo2Δ*) induces transcription of genes located at subtelomeric regions on chromosomes I and II²², similar to what we observed in cells lacking Endosulfine (*igo1Δ*) or Greatwall (*ppk18Δ cek1Δ*) after nitrogen starvation (Fig. 1a; Supplementary Fig. 1a; Supplementary Data 1, 2). This correlation prompted us to investigate whether Sgo2 levels might be altered in the *igo1Δ* mutant. Western-blot analysis revealed that *igo1*-deleted cells show a severe reduction of Sgo2 levels during entry into quiescence (Fig. 3a). As in the case of Rap1, reducing Pab1 levels in the *igo1Δ* mutant restored Sgo2 levels (Fig. 3b). To confirm the role of Igo1 in maintenance of Sgo2 levels and *knob* formation, we studied the localisation of Sgo2 during quiescence entry. Sgo2 protein was tagged with GFP and its localisation during nitrogen starvation was examined. As previously described, in the wild-type strain, Sgo2-GFP localised as nuclear dots in most cells, ranging from 1 to 3 dots per cell (Fig. 3c). In the *igo1Δ* mutant, we detected no significant differences with the wild-type in nitrogen-rich media ($t = 0$ h), only a slight decrease in dot size and brightness. However, when we shifted the cells to nitrogen-free media we observed a clear decrease in the number of dots per cell in the *igo1Δ* mutant (Fig. 3c). Knob colocalisation with Sgo2 was confirmed in wild-type and *igo1Δ* cells growing in nitrogen-rich media by SRRF microscopy (Supplementary Fig. 3a). In these cells, the brightest DAPI signal colocalised with the Sgo2-GFP signal. After 4 h of nitrogen starvation, the Sgo2-GFP signal became fragmented in wild-type cells but still colocalised with the *knob*. In most *igo1Δ* cells, the Sgo2 signal disappeared after 4 h of nitrogen starvation. In those cells where Sgo2 was detectable, we did not observe colocalization with the brightest

DAPI signal (Supplementary Fig. 3b). These data indicate that Igo1 is required for maintaining Sgo2 protein levels and for the formation of *knobs*, a structure essential for maintaining the transcriptional repression of subtelomeric genes.

Another key protein complex required for silencing subtelomeric regions is the heterochromatic repressor complex SHREC (Snf2-like/HDAC-containing repressor complex)^{32,33}, composed of Mit1, Clr1, Clr2, and Clr3. The SHREC complex plays regulatory roles in histone acetylation, as a chromatin remodeller and in the stability of subtelomeric nucleosomes^{27,32,33}. To determine if SHREC was also affected by PP2A activity, we examined Clr2 and Clr3 levels. In both cases, we detected a modest but reproducible decrease in protein levels during nitrogen starvation in the *igo1Δ* mutant (Fig. 3d, e). ChIP analysis showed that lack of Igo1 caused an increase in histone H3-K14 acetylation in the overexpressed subtelomeric genes SPCC977.15 and SPAC186.06 after 4 h of nitrogen starvation consistent with loss of SHREC function (Fig. 3f). Taken together, these results suggest that the Greatwall-Endosulfine-PP2A/B55 pathway modulates SH and ST chromatin organisation and subtelomeric gene silencing.

PP2A/B55 regulates translation through its physical and functional interaction with protein complexes involved in tRNA modification

Our data indicate that the *igo1Δ* mutant exhibits reduced levels of proteins essential for maintaining telomeric and subtelomeric organisation. However, what is the molecular mechanism underlying these phenotypes? We explored three possibilities: reduced protein stability, reduced transcription, or reduced translation.

To examine protein stability, we treated cells with cycloheximide and monitored Rap1 protein levels over time. After treatment with cycloheximide, Rap1 was degraded with similar kinetics in wild-type and *igo1Δ* cells (Supplementary Fig. 4a). Similarly, *rap1* mRNA levels were not reduced in *igo1Δ* cells; on the contrary, the *rap1* gene exhibited higher transcript levels in the *igo1Δ* mutant compared to wild-type cells (Supplementary Fig. 4b). Likewise, no significant changes in mRNA levels for *sgo2*, *clr2* or *clr3* in the *igo1Δ* mutant compared to the wild-type (Supplementary Fig. 4c) indicating that transcription is not responsible for the decrease in protein levels.

Evidence of a translation defect in the *igo1Δ* mutant was obtained by mass-spectrometry analysis of proteins co-purifying with the PP2A/Pab1 protein phosphatase. Paa1, the structural subunit of the PP2A complex, was tagged with YFP and expressed from its endogenous promoter at its chromosomal locus. After one hour of nitrogen starvation, Paa1-YFP was pulled down and co-purifying proteins were analysed by mass-spectrometry. Our results revealed the presence of all components of PP2A protein complexes including Paa1, the catalytic subunits Ppa1, Ppa2, and Ppa3, and the regulatory subunits Pab1, Par1 and Par2 (Supplementary Data 4). Additionally, several PP2A regulators (Igo1, Zds1, Dis2, Ppe1 and Ekc1) and components of the PP2A SIP/STRIPAK complex³⁴ were also detected, confirming that the pull-down approach was successful.

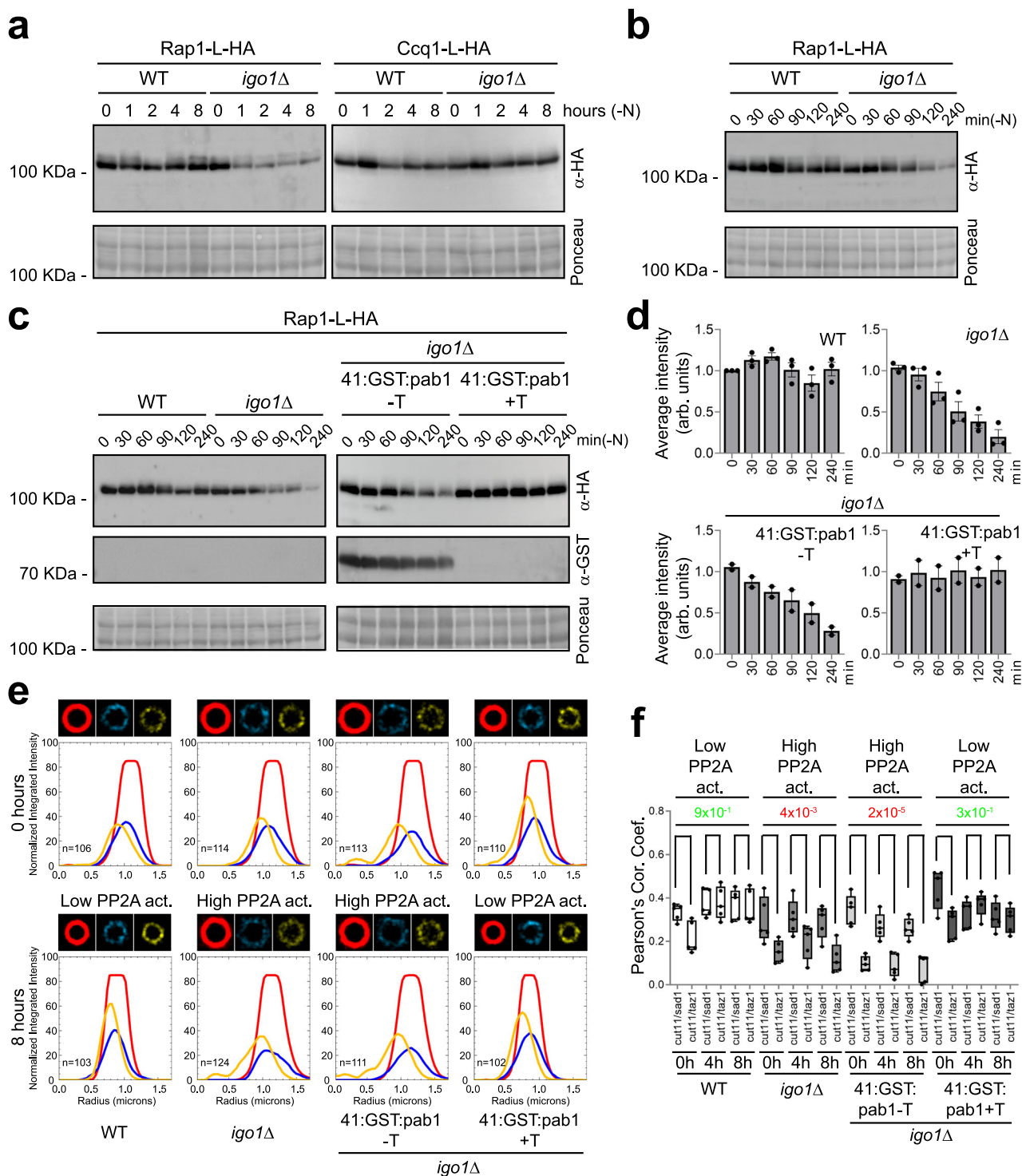
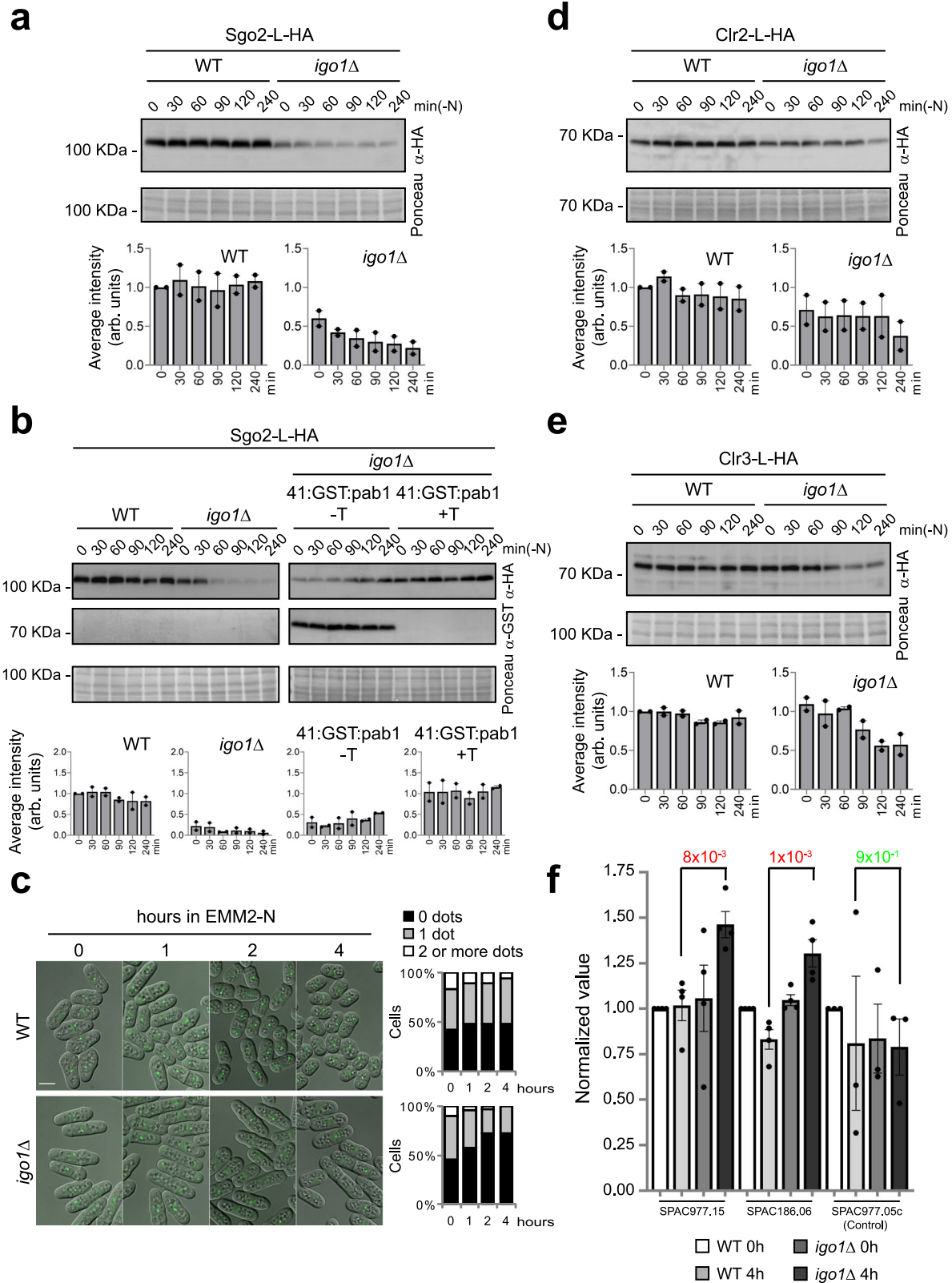


Fig. 2 | Telomeric detachment from the nuclear envelope in *igo1Δ* cells is mediated by reduced Rap1 protein levels. **a** Extracts from *rap1::HA* and *ccq1::HA* cells in a WT and *igo1Δ* background were collected at 0, 1, 2, 4 and 8 h of nitrogen starvation. These extracts were analysed by SDS-PAGE and western blotting using anti-HA antibodies. Ponceau staining was used as the loading control. **b** Extracts from *rap1::HA* cells in a WT and *igo1Δ* background, collected every 30 min during the first 2 h and then at 4 h of nitrogen starvation. These extracts were analysed by SDS-PAGE and western blotting using anti-HA antibodies. Ponceau staining was used as the loading control. **c** Extracts from *rap1::HA* and *rap1::HA Pnm41x:GST:pab1* cells in a WT and *igo1Δ* background were collected during nitrogen starvation and analysed by SDS-PAGE and western blot using anti-HA and anti-GST antibodies. Strains were grown with or without thiamine (+T or -T) to repress or induce the *pab1* gene, encoding the B55 regulatory subunit of PP2A. Ponceau staining was used as the loading control. **d** Immunoblot quantification of

c was performed using Image Studio Lite software, $n = 3$ of a total of 8 for *igo1Δ*, $n = 2$ of a total of 6 for *igo1Δ Pnm41x:GST:pab1*. Data are presented as the mean \pm S.E.M. **e** Radial Profile Analysis of WT, *igo1Δ* and *igo1Δ Pnm41x:GST:pab1* cells bearing Cut11 (in red), Sad1 (in cyan) or Taz1 (in yellow) in EMM2 (0 h) and after 8 h of nitrogen starvation. The *igo1Δ Pnm41x:GST:pab1* cells were grown with or without thiamine (+T or -T) to repress or induce the expression of *pab1*. Over 100 nuclei were projected to generate the images and graphics, $n = 3$. **f** Colocalisation between Cut11/Sad1 and Cut11/Taz1 signals of **e** was quantified as Pearson correlation coefficients using ImageJ software. ANCOVA p -values are indicated, significant differences are shown in red. The box extends from the 25th to the 75th percentiles, with the horizontal line indicating the median. The whiskers extend to the minimum and maximum values. $n = 5$ (with at least 20 nuclei analysed per assay). Raw gel images are provided in Supplementary Fig. 9. Source data are provided as a Source data file.



The mass-spectrometry analysis also showed an over-representation of proteins related to ribosome structure, translation initiation, aminoacylation, and tRNA modification in the Paa1 interactome (Fig. 4a; Supplementary Fig. 5a). We focused on Trm112, a widely conserved protein with a crucial role in translation. Specifically, Trm112 regulates methyltransferase enzymes (Trm9, Trm11, Mtq2 and Bud23) during ribosome biogenesis, tRNA modification and stop

codon recognition^{35,36}. We confirmed an interaction between Trm112 and the PP2A-Pab1 complex by repeating the mass-spectrometry analysis using Pab1, the B55 regulatory subunit of the PP2A complex, as bait. Trm112 was pulled down as an interacting partner of PP2A/Pab1 (Fig. 4a; Supplementary Fig. 5b; Supplementary Data 5). The Paa1-Trm112 interaction was further validated by co-immunoprecipitation, showing a stronger association in nitrogen-depleted than in

Fig. 3 | Crucial proteins required for silencing subtelomeric gene expression are downregulated in *igo1Δ* cells. **a** Extracts from *sgo2::L:HA* cells in a WT and *igo1Δ* backgrounds were collected every 30 min during the first 2 h and then at 4 h of nitrogen starvation. These extracts were analysed by SDS-PAGE and western blotting using anti-HA antibodies. Ponceau staining was used as the loading control. Immunoblot quantification was performed using Image Studio Lite software, $n = 2$ of a total of 4 for *igo1Δ*. Data are presented as the mean \pm S.E.M. **b** Extracts from strains bearing *sgo2::L:HA* or *sgo2::L:HA P_{nmt41}:GST:pab1*, were analysed by SDS-PAGE and western blotting with anti-HA and anti-GST antibodies. The *igo1Δ P_{nmt41}:GST:pab1* cells were grown with or without thiamine (+T or -T) to repress or induce the expression of *pab1*. Ponceau staining was used as the loading control. Immunoblot quantification was performed using Image Studio Lite software, $n = 2$ of a total of 4 for *igo1Δ*, $n = 2$ of a total of 6 for *igo1Δ P_{nmt41}:GST:pab1*. Data are presented as the mean \pm S.E.M. **c** Representative micrographs of WT or *igo1Δ* cells expressing *sgo2::L:GFP* during entry into quiescence. The overlay of fluorescence

and DIC images is shown. Quantification was carried out using ImageJ software from two independent experiments involving more than 150 cells. Bar: 5 μ m. **d** Similar to **(a)**, *clr2::L:HA* protein was analysed in both WT and *igo1Δ* backgrounds. Immunoblot quantification was performed using Image Studio Lite software, $n = 2$. Data are presented as the mean \pm S.E.M. **e** Similar to **(a)**, *clr3::L:HA* protein was analysed in both WT and *igo1Δ* backgrounds. Immunoblot quantification was performed using Image Studio Lite software, $n = 2$. Data are presented as the mean \pm S.E.M. **f** ChIP-qPCR was performed with anti-H3K14-acetyl antibodies and quantified with primer pairs at the indicated ORFs. WT and *igo1Δ* cells grown in nitrogen-rich media (EMM2) or after 4 h of nitrogen starvation were analysed. The graphs represent normalized values, and error bars (SEM) for all ChIP-qPCR experiments were calculated from at least biological triplicates ($n \geq 3$). A two-way ANOVA was performed, p -values are indicated, with significant differences shown in red. For gel source data, see Supplementary Fig. 9. Source data are provided as a Source data file.

nitrogen-rich media (Fig. 4b). Interestingly, several subunits of the Elongator complex (Elp1, Elp2 and Elp3) were also pulled down as interacting partners of PP2A/Pab1 when Pab1 was slightly over-expressed from the *nmt41* promoter (Fig. 4a; Supplementary Fig. 5c; Supplementary Data 6). The Pab1-Elp3 interaction was also validated by co-immunoprecipitation in cells expressing wild-type levels of Pab1 (Fig. 4b).

The Elongator complex, along with Trm112/Trm9 and the Ctu1/Ctu2 complexes, plays a critical role in the formation of the 5-methoxycarbonylmethyl (mcm⁵) and 5-methoxycarbonylmethyl-2-thiouridine (mcm⁵s²) side chains on uridine 34 (U₃₄) at the tRNA wobble position during vegetative growth and under stress conditions^{8,12,13,37–40}. We conducted an analysis of Trm112 protein levels during nitrogen starvation in both wild-type and *igo1*-deleted cells. In the wild-type, Trm112 levels remained constant during the first two hours and then exhibited a slight decrease after four hours. In contrast, in the *igo1Δ* mutant, we observed a more pronounced reduction in Trm112 protein levels during entry into quiescence (Fig. 4c, left panel). The *trm112* transcript levels were similar in wild-type and *igo1Δ* mutant cells (Supplementary Fig. 4c). Interestingly, as shown previously for other proteins, the reduction of PP2A/B55 activity restored Trm112 protein levels (Fig. 4c, right panel). We also found that the levels of Ctu1 protein, which cooperates with Ctu2 in tRNA U₃₄ thiolation^{41,42}, were also diminished in the *igo1Δ* background (Fig. 4d), whereas the *ctu1* mRNA showed a similar pattern to the wild-type (Supplementary Fig. 4c). The catalytic subunit of Elongator (Elp3) was not regulated at the level of mRNA or protein (Supplementary Fig. 4d, e).

Collectively, these data suggest potential impairment of tRNA modifications in the *igo1Δ* mutant. To assess this possibility, we tested the sensitivity of the *igo1Δ* mutant to drugs that affect translation, such as paromomycin, puromycin or cycloheximide, in both nitrogen-rich (EMM2) and nitrogen-poor (MMPhe) media. Among all the drugs tested, only paromomycin, which induces codon misreading⁴³, exhibited an effect on the *igo1Δ* mutant (Fig. 4e), particularly in MMPhe.

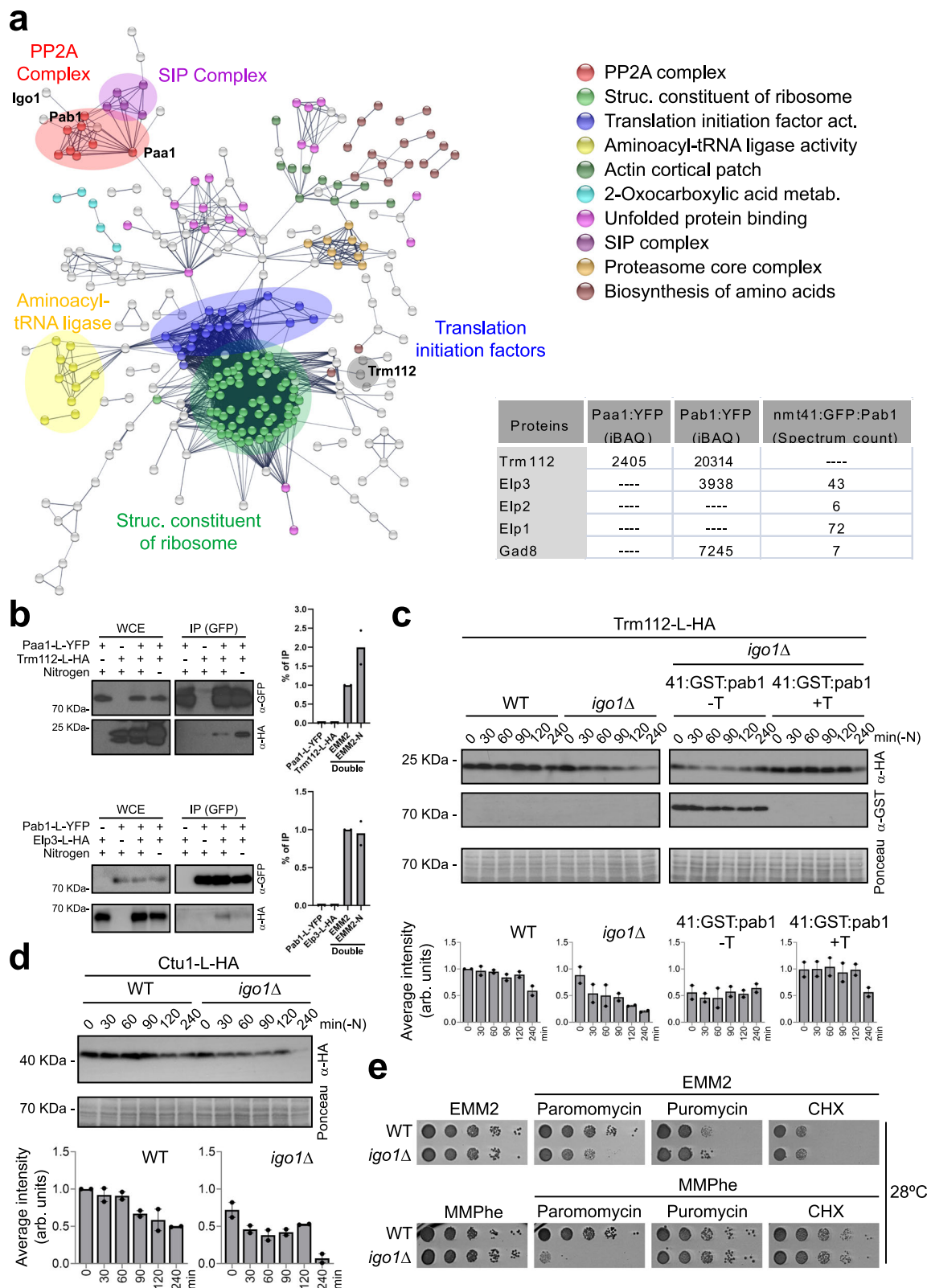
In summary, our data indicate a potential role for the Greatwall-Endosulfine-PP2A/B55 pathway in regulating translation during the onset of quiescence, probably involving tRNA modifications that enhance codon-anticodon recognition.

The *igo1Δ* mutant is defective in U₃₄ and A₃₇ tRNA modifications

In all organisms, modifications of uridine 34 at the wobble position (U₃₄) of certain tRNAs are necessary to enhance codon-anticodon recognition³⁷. These modifications are mediated by the Elongator complex, which introduces an acetyl group at position 5 of U₃₄ (cm⁵U₃₄), the Trm112/Trm9 methyltransferase complex involved in the formation of mcm⁵U₃₄, and the Ctu1-Ctu2 complex, which catalyses the thiolation at carbon 2 of U₃₄ (mcm⁵s²U₃₄) (Supplementary Fig. 6a).

Previous studies in *S. pombe* have reported that differences in codon usage and tRNA epitranscriptome play a crucial role in regulating translation efficiency during the cell cycle and under oxidative stress. The mRNAs of the cell cycle regulator Cdr2³⁹ and of the stress-responsive transcription factors Atf1 and Pcr1^{12,13} exhibit a high usage of lysine AAA (AAA_{lys}) codons compared to AAG (AAG_{lys}) codons, and their translational rate is particularly sensitive to deficiencies in tRNA modifications mediated by the Elongator, Trm112/Trm9 and Ctu1/Ctu2 complexes^{8,12,13,39}. Therefore, we hypothesised that differences in AAA_{lys} codon usage might be responsible for the translation phenotype observed in the *igo1Δ* mutant. To test this hypothesis, we examined the use of AAA_{lys} versus AAG_{lys} codons for some of the proteins analysed in our study and found that all the proteins defective in the *igo1Δ* mutant (Rap1, Sgo2, Clr3, Clr2, and Ctu1) primarily utilise the AAA_{lys} codon (Supplementary Fig. 6b). Proteins with reduced AAA_{lys} codon usage, such as Ccq1, Pgk1, Krs1, or Swi6, did not exhibit translation deficiencies during nitrogen starvation in the *igo1Δ* mutant (Fig. 2a; Supplementary Fig. 6b, c).

To confirm the potential defect in U₃₄ tRNA modification in the *igo1Δ* mutant, we employed quantitative liquid chromatography coupled to mass spectrometry (LC-MS)⁸ to analyse tRNAs extracted from wild-type and *igo1Δ* cells. Samples were collected during exponential growth and at 2 and 4 h of nitrogen starvation. This analysis revealed an increase in most of the tRNA modifications in wild-type cells upon entry into quiescence, in particular mcm⁵s²U₃₄ levels. However, in the *igo1Δ* mutant, most of the tRNA modifications diminished after 4 h of nitrogen starvation, especially mcm⁵s²U₃₄ levels (Fig. 5a, b; Supplementary Fig. 6d, e). Furthermore, this analysis also indicated a 20–25% reduction in A₃₇ N⁶-threonylcarbamoyladenosine (t⁶) modification in the *igo1Δ* mutant (Fig. 5a; Supplementary Fig. 6d–f). The t⁶A₃₇ tRNA modification, present in Archaea and Eukarya, mediated by the protein Sua5 and the KEOPS/EKC complex, is essential for cell growth and accurate translation^{44–46}. Once again, we hypothesised that differences in AAA_{lys} codon usage might be responsible for the reduction in t⁶A₃₇ modification in the *igo1Δ* mutant. When we examined the use of AAA_{lys} versus AAG_{lys} codons for Sua5 and the KEOPS/EKC subunits, we found that Pcc1 and Cgi121 (two components of KEOPS/EKC complex) primarily use the AAA_{lys} codons (Supplementary Fig. 6g). Taking Cgi121 as an example, we detected a significant reduction in Cgi121 level in the *igo1Δ* mutant during nitrogen starvation (Supplementary Fig. 6h). These data suggest that a defect in the translation of Cgi121 protein could be responsible of the reduction in t⁶A₃₇ tRNA modification in the *igo1Δ* mutant. Both mcm⁵s²U₃₄ and t⁶A₃₇ modifications are involved in decoding codons that start with adenosine, promoting codon-anticodon pairing and enhancing translation fidelity^{47,48}. These findings provide a molecular explanation for the paromomycin hypersensitivity and translation defect observed in the *igo1Δ* mutant under nitrogen-stress conditions (Fig. 4e).



As cells enter quiescence, a notable reduction in tRNA^{Lys}_{UUU} levels was observed in both wild-type and *igo1Δ* cells (Supplementary Fig. 7a), suggesting that this tRNA becomes limiting in quiescent cells. Previous studies in yeast and worms have shown that over-expression of tRNAs can effectively restore translation rates and protein homeostasis in mutants defective in tRNA modification^{8,12,13,39,47}. Using Rap1 as an example, we assessed whether over-expression of tRNA^{Lys}_{UUU}

would lead to recovery of Rap1 protein levels in the *igo1Δ* mutant, with tRNA^{Lys}_{CUU} over-expression serving as a control. As anticipated, over-expression of tRNA^{Lys}_{CUU} had no impact on Rap1 levels, while over-expression of tRNA^{Lys}_{UUU} partially restored Rap1 protein levels (Supplementary Fig. 7b) and alleviated the telomere detachment phenotype in nitrogen-starved *igo1Δ* cells (Supplementary Fig. 7c). To confirm that the reduced levels of Rap1 protein in *igo1Δ* cells resulted

Fig. 4 | PP2A interacts with proteins involved in tRNA modification.

a Interacting network resulting from mass-spectrometry analysis for *paal1::YFP* in EMM2-N. Cellular processes or protein complexes with a significant enrichment are colour-coded. Two experimental replicas of the mass spectrometry were performed, $n = 2$. Extracts from the untagged wild-type strain were used as negative control in the immunopurification experiment. Summary table showing the main PP2A interactors analysed in this manuscript. **b** top, Interaction between *Paal1::YFP* and *Trm112::HA*. Protein extracts from cells expressing *paal1::YFP*, *trm112::HA* or *paal1::YFP trm112::HA* cultured in nitrogen-rich or nitrogen-depleted media were immunoprecipitated with anti-GFP beads and probed with anti-GFP and anti-HA antibodies. Extracts (WCE) were assayed for levels of *paal1::YFP* and *trm112::HA* by western blot. Bottom, Interaction between *Pab1::YFP* and *Elp3::HA*. Protein extracts from cells expressing *pab1::YFP*, *elp3::HA* or *pab1::YFP elp3::HA* cultured in nitrogen-rich or nitrogen-depleted media were immunoprecipitated with anti-GFP beads and probed with anti-GFP and anti-HA antibodies. Extracts (WCE) were assayed for levels of *Pab1::YFP* and *Elp3::HA* by western blot. $n = 2$. Data are presented as the mean \pm S.E.M. **c** Extracts from cells expressing *trm112::HA* or

trm112::HA P_{nmc4}Ix::GST:pab1, were analysed by SDS-PAGE followed by immunoblotting with anti-HA and anti-GST antibodies. The *igo1Δ P_{nmc4}Ix::GST:pab1* cells were grown in EMM2 with or without thiamine (+T or -T) to repress or induce the expression of *pab1*. Ponceau staining was used as the loading control. Immunoblot quantification was performed using Image Studio Lite software, $n = 2$ of a total of 4 for *igo1Δ*, $n = 2$ of a total of 6 for *igo1Δ P_{nmc4}Ix::GST:pab1*. Data are presented as the mean \pm S.E.M. **d** Extracts from *Ctu1::HA* cells in a WT and *igo1Δ* backgrounds were collected every 30 minutes during the first 2 h and then at 4 h of nitrogen starvation. These extracts were analysed by SDS-PAGE and immunoblotting using anti-HA antibodies. Ponceau staining was used as the loading control. Immunoblot quantification was performed using Image Studio Lite software, $n = 2$ of a total of 4 for *igo1Δ*. Data are presented as the mean \pm S.E.M. **e** Serial dilutions from WT and *igo1Δ* cultures were spotted onto EMM2 (Minimal Media containing NH₄Cl) or MMPhe (Minimal Media containing Phenylalanine) plates without or with paromomycin (0.5 mg/ml), puromycin (0.5 mg/ml) or cycloheximide (CHX, 2.5 μg/ml). For gel source data, see Supplementary Fig. 9. Source data are provided as a Source data file.

from defective translation of its mRNA, we engineered a mutant version of the *rap1* gene in which the 40 AAA codons were substituted with AAG, making all lysine codons independent of tRNA modification. Consistent with previous findings for other proteins, the translation deficiency of Rap1 in the *igo1Δ* mutant was completely rescued by expressing the *rap1-allaag* allele (Fig. 5c). Similarly, expression of the *ctu1-allaag* allele restored Ctu1 protein levels in nitrogen-starved *igo1Δ* cells (Supplementary Fig. 7d).

To confirm a translation defect in the *igo1Δ* mutant, we performed polysome analyses using sucrose gradient fractionation of extracts obtained from exponentially growing (+Nitrogen) and nitrogen-starved (-Nitrogen) wild-type and *igo1Δ* cells. In the *igo1Δ* mutant, we observed a reduction to 78% in the polysome/monosome ratio in cells growing in nitrogen-rich media compared to the wild-type (Fig. 5d), which decreased further to 27% after 4 h of nitrogen starvation (Fig. 5e). We pooled the non-translated or poorly translated fractions (NT) and the polysome fractions (P) of the gradient and determined the mRNA levels of *rap1* and *ctu1*, two mRNAs with high AAA_{lys} codon bias, and *fil1* and *act1*, two mRNAs with low AAA_{lys} codon bias. This analysis revealed a reduction in translation to 40% for *rap1* and 30% for *ctu1*, while *fil1* and *act1* were hardly affected (Fig. 5e).

In summary, considering all the data, we conclude that during the transition into quiescence, Endosulfine Igo1 is necessary for facilitating U₃₄ and A₃₇ tRNA modifications. These modifications are crucial for enhancing the translation efficiency and fidelity of proteins encoded by mRNAs with a high usage of AAA_{lys} codons.

Gad8 phosphorylation is required to enhance translation during quiescence entry

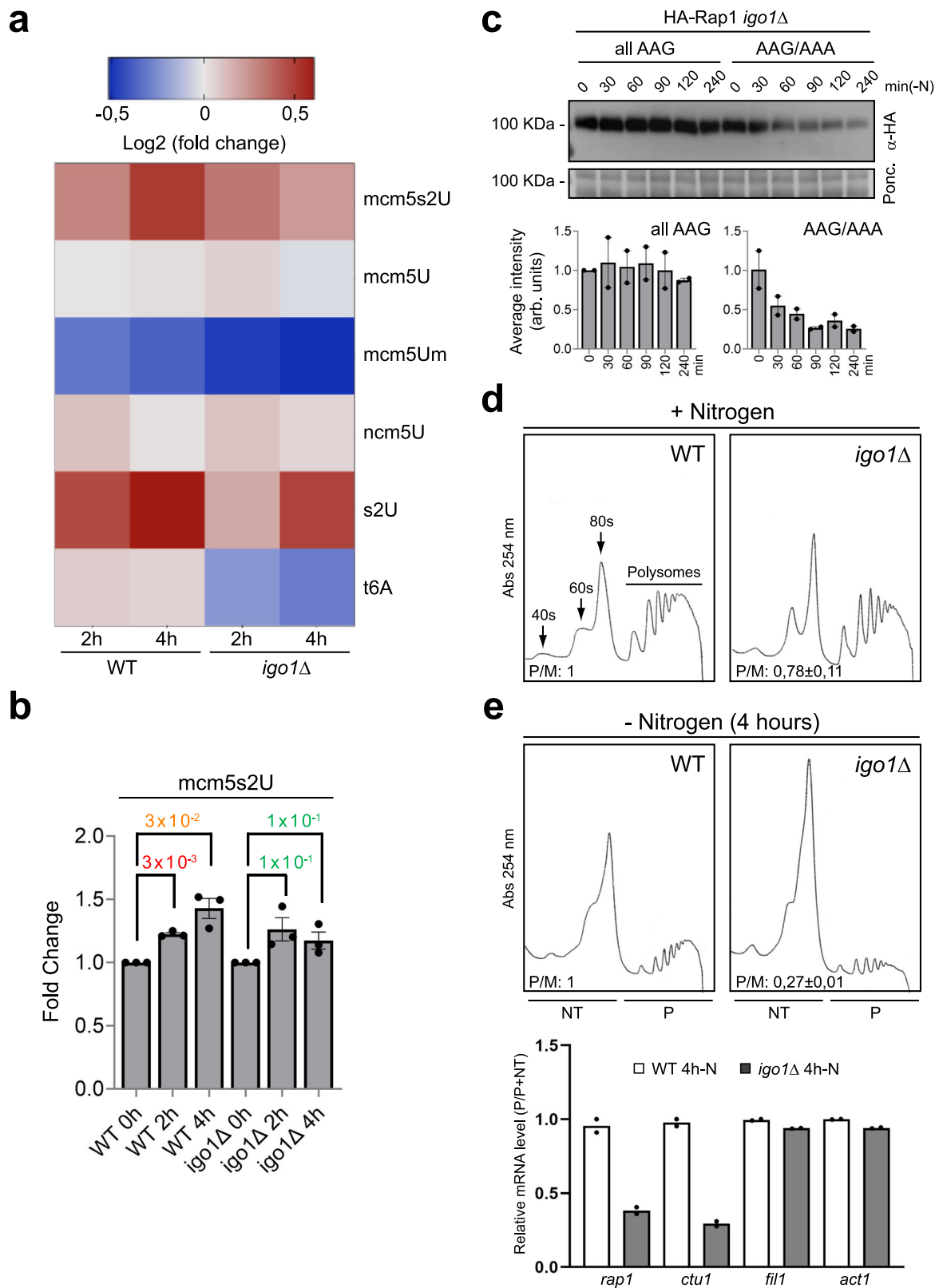
We then investigated the underlying molecular mechanism that triggers the translational defect due to a failure in tRNA modification. We identified Gad8 as an interactor of PP2A/Pab1 (Fig. 4a; Supplementary Data 5, 6). Previous studies demonstrated that PP2A/Pab1 counteracts the phosphorylation of Gad8 by TORC2 at serine 546, suggesting that Gad8 is a direct target of PP2A/Pab1^{6,7}. Additionally, active Gad8 phosphorylated at S546 activates Elongator by inhibiting Gsk3, a glycogen synthase kinase that inhibits Elongator by phosphorylating the Elp4 subunit at serine 114⁸.

These findings prompted us to investigate the potential role of Igo1 in Gad8 phosphorylation during quiescence entry. Notably, it has previously been reported that deletion of *elp3*, which encodes the tRNA acetyltransferase subunit of the Elongator complex, leads to a reduction in Gad8 protein levels⁸. A sequence analysis of the *gad8* mRNA revealed a high usage of AAA_{lys} codons, like *rap1* (Supplementary Fig. 6b, *gad8* z-score_{AAA/AAG} = 0.73/-0.73 vs. *rap1* z-score_{AAA/AAG} = 0.72/-0.71). This observation led us to investigate whether high PP2A/B55 activity, in the absence of Igo1, could be relevant for

maintaining Gad8 protein levels during nitrogen starvation. Western blot analysis clearly showed a decrease in Gad8 protein levels in the *igo1Δ* mutant (Fig. 6a). Furthermore, the phosphorylation status of Gad8 at S546 was also reduced in the absence of Igo1, compared to wild-type cells (Fig. 6b). In addition, we observed a reduction in *gad8* mRNA levels in *igo1Δ* cells compared to the wild-type (Supplementary Fig. 4c), suggesting that Gad8 is regulated at multiple levels: transcription, translation and phosphorylation. These results suggest that during nitrogen starvation, inhibition of PP2A/Pab1 leads to the accumulation of phosphorylated Gad8 at S546 by TORC2 and consequent activation of the Elongator complex. This mechanism generates a positive feedback loop that enhances translation of Gad8 and promotes more U₃₄ tRNA modifications (see Fig. 7).

If our model is correct, and PP2A/B55 indeed regulates Elongator activity through Gad8 protein homeostasis, the deletion of the *gad8* gene should lead to a substantial decrease in proteins with high AAA_{lys} codon usage. To test this hypothesis, we examined the levels of Sgo2, a protein with a very high AAA_{lys} codon usage (z-score_{AAA/AAG} = 1.28/-1.28), in a *gad8Δ* mutant background. Western blot analysis showed a reduction in Sgo2 protein levels in the *gad8Δ* mutant (Fig. 6c). As a positive control, we used the *elp3Δ* mutant, where the reduction in Sgo2 levels was even greater (Fig. 6d). Moreover, both *gad8Δ* and *elp3Δ* mutants displayed sensitivity to paromomycin in both nitrogen-rich and nitrogen-poor media (Supplementary Fig. 7e), although the sensitivity to paromomycin in nitrogen-poor medium was more pronounced in the *igo1Δ* mutant (Fig. 6e; Supplementary Fig. 7e). Thus, our data strongly suggests that defects in the Elongator activation pathway led to decreased translation efficiency of mRNAs with high AAA_{lys} codon usage.

Finally, to confirm the connection between Igo1 and the Elongator activation pathway, we generated a double mutant, *igo1Δ gsk3Δ*. Gsk3 is an Elongator inhibitor in *S. pombe*⁸. As mentioned earlier, the *igo1Δ* mutant exhibited sensitivity to paromomycin, particularly in nitrogen-poor media containing phenylalanine (Fig. 4e). If this phenotype is indeed related to reduced Elongator activity, the *igo1Δ gsk3Δ* double deletion should rescue this defect. Wild-type, *igo1Δ* and *gsk3Δ* single mutants, along with the *igo1Δ gsk3Δ* double mutant, were cultivated in nitrogen-poor (MMPhe) medium with or without paromomycin, and their growth phenotype was assessed. The *igo1Δ* mutant displayed hypersensitivity to paromomycin, while the *gsk3Δ* mutant exhibited mild resistance compared to the wild-type strain. A partial improvement in cell growth in the presence of paromomycin was detected in the *igo1Δ gsk3Δ* double mutant clones compared to the *igo1Δ* mutant (Fig. 6e). As mentioned earlier, Gsk3 inhibits Elongator by phosphorylating the Elp4 subunit at serine 114⁸. Expression of *elp4-S114A* partially rescued the paromomycin sensitive phenotype of the *igo1Δ* mutant (Supplementary Fig. 7f).



These findings suggest that proper Igo1-mediated activation of Elongator is crucial for maintaining the rate of translation during quiescence entry.

Discussion

Entry into quiescence in yeasts is regulated by diverse signalling cascades that converge on the Greatwall-Endosulfine-PP2A/B55

pathway^{3,5,49–51}. In *S. pombe*, the primary signal regulating entry into quiescence is nitrogen starvation, which reduces the TORC1 activity and increases TORC2 activity^{4,6,7,52–58}. The inactivation of TORC1 results in reduced protein synthesis and the activation of protein degradation through autophagy. However, quiescent cells must maintain a continuous supply of specific proteins to remain viable.

Fig. 5 | Igo1 regulates tRNA modifications. **a** Heat map (\log_2 fold-change) analysis from three biological replicates of the relative levels of tRNA ribonucleoside modifications in WT and *igo1Δ* cells. The side colour bar displays the range of \log_2 (fold-change) values. The heat map shows changes at 2 and 4 h of nitrogen starvation compared to exponentially growing cells ($t = 0$), with the *igo1Δ* mutant showing a decrease in $mcm^5s^2U_{34}$ and t^6A_{37} modification relative to the WT. **b** Fold-change values of $mcm^5s^2U_{34}$ modification in WT and *igo1Δ* mutant cells. A two-way ANOVA was performed, p -values were calculated from biological triplicates, with significant differences shown in red and orange. Data are presented as the mean \pm S.E.M. **c** Extracts from *igo1Δ* mutant cells transformed with episomal plasmids $P_{nmt4Ix:HA:rap1}$ (AAA/AAG) or mutated version $P_{nmt4Ix:HA:rap1}$ (all AAG) were analysed by SDS-PAGE followed by immunoblotting with anti-HA antibodies during nitrogen starvation. Ponceau staining was used as a loading control. Immunoblot quantification was performed using Image Studio Lite software, $n = 2$ of a total of 4 for *igo1Δ*. Data are presented as the mean \pm S.E.M. **d** Polysome analysis using

sucrose gradient fractionation of WT and *igo1Δ* extracts from cells cultured in EMM2 (+ Nitrogen). Two replicates of the experiment were performed and the polysome/monosome ratio (P/M ratio) was calculated. **e** Polysome analysis using sucrose fractionation of WT and *igo1Δ* extracts from cells cultured in EMM2 lacking nitrogen for 4 h (-Nitrogen 4 h). Two replicates of the experiment were performed and the polysome/monosome ratio (P/M ratio) was calculated. Total RNA was purified from the different fractions, resuspended in DEPC- H_2O , combining RNA from two consecutive fractions. cDNA was synthesised and pooled into, non-translating/poorly translating mRNAs (NT), corresponding to mRNAs associated to low molecular weight fractions, free ribosomal subunits and vacant ribosomes, and actively translating mRNAs found associated with the polysomal fractions (P). The mRNA levels (P/P + NT) for *rap1*, *ctu1*, *fill* and *act1* were determined in the *igo1Δ* mutant relative to the WT, with an assigned value of 1 by qPCR. Source data are provided as a Source data file.

In this study, we demonstrate that the Greatwall-Endosulfine-PP2A/B55 pathway links the inactivation of TORC1 with the activation of TORC2 signalling to promote the activation of the Elongator complex and other tRNA modification complexes essential for sustaining the translation programme during the transition into quiescence. This is achieved by facilitating U_{34} and A_{37} tRNA modifications, which enhance translation efficiency and fidelity of key proteins, including those required for telomeric and subtelomeric functions.

The reduction of PP2A/B55 activity, achieved through the activation of Greatwall and Endosulfine, is necessary for the accumulation of phosphorylated Gad8 at S546⁷. This phosphorylation event enhances the activity of the Elongator complex by inhibiting glycogen synthase kinase (Gsk3)⁸. Increased Elongator activity promotes the efficient translation of mRNAs with high AAA_{lys} codon usage, including *tsc2* (an inhibitor of TORC1)⁸, *gad8* (a positive effector of TORC2), *trm112*, *ctu1* and *cgi121* (involved in U_{34} and A_{37} tRNA modifications) (Fig. 7). All of these generate feedback loops that facilitate the switch from high TORC1 to high TORC2 activity, promoting the translation of Elongator-tunable transcripts as cells enter quiescence. Furthermore, the synthesis of key proteins involved in telomeric and subtelomeric organisation, such as Rap1, Sgo2, Clr2 or Clr3, which also exhibit high AAA_{lys} codon usage, depends on the proper activation of Elongator. Therefore, we outline the complete pathway connecting the nutritional environment - specifically the balance between TORC1 and TORC2 - to the modulation of tRNA modifications and translation, thereby maintaining protein homeostasis during the transition from proliferation to quiescence.

Previous studies have demonstrated that the deletion of *rap1* (encoding a component of the shelterin complex) or *bqt4* (encoding a component of the bouquet complex) causes telomeric detachment from the NE^{23,25,26}. Our findings suggest that the telomeric detachment defect in the *igo1Δ* mutant is probably caused by a reduction in Rap1 protein levels (Fig. 2a–d). Interestingly, Bqt4, the other protein that creates a molecular link between telomeres and the NE, has a low AAA_{lys} codon usage ($z\text{-score}_{AAA/AAG} = -0.94/0.95$), making it unlikely to be responsible for the telomeric detachment phenotype in the *igo1Δ* mutant. However, other proteins may be involved in the telomeric attachment to the NE, such as Lem2, a member of the Lap2/Emerin/Man1 (LEM) family of lamin-associated proteins, which is known to be involved in telomere anchoring and heterochromatic gene silencing^{59–61}. Lem2 mRNA has a high AAA_{lys} codon usage (30 AAA, 9 AAG, $z\text{-score}_{AAA/AAG} = 0.88/-0.88$), suggesting that it may also be subject to translation defects in the *igo1Δ* mutant. Western blot analysis revealed that nitrogen-starved *igo1Δ* cells show a significant reduction in Lem2 protein levels (Supplementary Fig. 8a). This finding suggests that not only Rap1 but also Lem2 could contribute to the telomeric detachment phenotype in the *igo1Δ* mutant (Fig. 7).

In addition to the telomeric anchoring defect, the *igo1Δ* mutant exhibited upregulation of genes located in the subtelomeric regions of

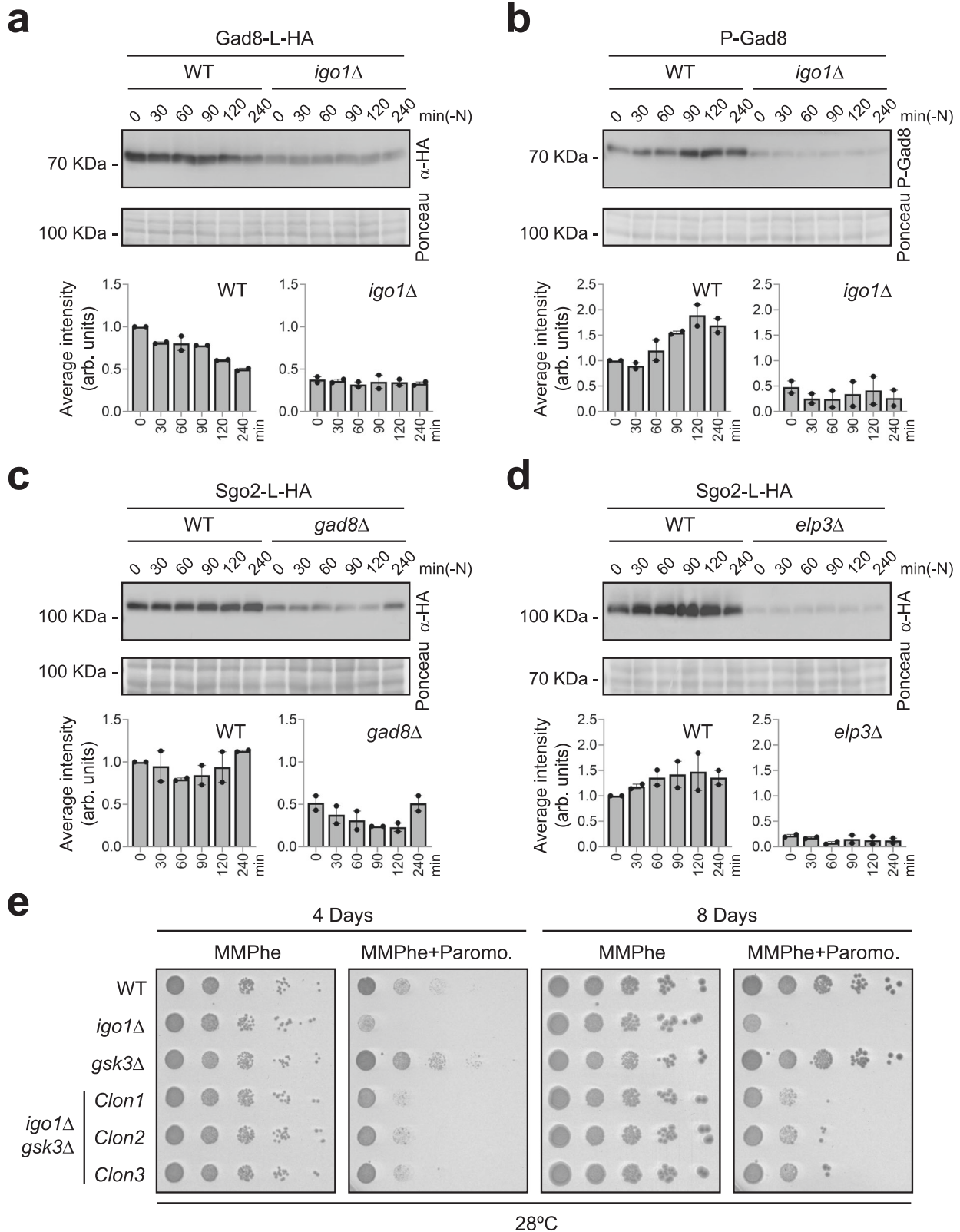
chromosomes I and II (Fig. 1a; Supplementary Fig. 1a). Several proteins related to subtelomeric organisation were defective in the *igo1Δ* background, particularly Sgo2, whose protein levels were significantly reduced (Fig. 3a). Sgo2 plays a role in *knobs* assembly, and its deletion leads to derepression of genes located in subtelomeric regions^{21,22}. Our data demonstrate that Igo1 is involved in *knobs* assembly, and its deletion results in defects in the regulation of subtelomeric genes. The overlapping roles and phenotypes between Sgo2 and Igo1 suggest that the reduction in Sgo2 protein levels is responsible for the derepression of subtelomeric genes in the *igo1Δ* mutant. However, other proteins, such as Clr2 or Clr3, which are involved in silencing could also contribute to this phenotype.

All the proteins tested in our study had their levels restored after reducing PP2A/B55 activity, indicating that low PP2A/B55 activity was necessary to maintain protein homeostasis during quiescence entry. But what is the link between PP2A/B55 activity, translation and the telomeric/subtelomeric organisation?

Previous research has shown that deleting specific components of TORC2 signalling, such as *tor1* or *gad8*, leads to a significant derepression of genes located in subtelomeric regions⁶². However, the molecular mechanism linking these processes remained unclear. Our data reveal that not only components of the TORC2 complex but also elements acting downstream of the TORC1 complex, such as Greatwall (Ppk18 and Cek1) or Endosulfine (Igo1), play a crucial role in regulating subtelomeric gene expression. These findings establish a connection between the Greatwall-Endosulfine-PP2A/B55 pathway and telomeric/subtelomeric organisation.

A link between the TORC2 signalling pathway, the Elongator complex, and tRNA modifications has been demonstrated⁸. Our data further demonstrate that this connection is particularly relevant during entry into quiescence by elucidating the molecular details linking nitrogen starvation, TORC1 inactivation, activation of Greatwall-Endosulfine, inactivation of PP2A/Pab1, activation of Gad8, and upregulation of tRNA-modifying complexes (Fig. 7). Indeed, these molecular events affect not only the Elongator complex but also other tRNA modifiers, such as Trm112 or Ctu1. These interactions create positive feedback loops that are responsible for the transition from high TORC1 to high TORC2 activity, subsequently leading to further tRNA modifications. Mutations in Greatwall (Ppk18 and Cek1) or Endosulfine (*igo1*) result in a defect in this transition, causing a failure in tRNA modifications that affect the translation of mRNAs with a high AAA_{lys} codon usage encoding for proteins such as Rap1, Lem2, Sgo2, Clr2 and Clr3. This, in turn, triggers telomeric detachment and the derepression of subtelomeric genes.

In addition to the $mcm^5s^2U_{34}$ defect, we also observed a 20–25% reduction in t^6A_{37} in the Endosulfine (*igo1Δ*) mutant (Fig. 5a). These two closely located tRNA modifications play a crucial role in ensuring accurate codon-anticodon interactions by stabilising codon-anticodon pairings^{63–66}. Interestingly, $tRNA^{Lys}_{UUU}$ carries both the $mcm^5s^2U_{34}$ and



t^6A_{37} modifications, both of which are defective in the Endosulfine (*igo1* Δ) mutant. This finding provides an explanation for the strong sensitivity of *igo1* Δ cells to paromomycin compared to mutants in Elongator (*elp3* Δ) or Gad8 (*gad8* Δ). The defect in the t^6A_{37} modification could be explained by a reduction in Cgi121 protein levels, one of the subunits of the KEOPS complex responsible for this modification^{48,64}, which is encoded by an mRNA with a high AAA_{lys} codon usage.

Finally, an interesting concept has emerged over the last few years on tRNA modifications and stress, known as tRNA modification tunable transcripts (MoTTs). These transcripts are characterised by a specific use of degenerate codons and codon biases to encode essential stress response proteins. Translation of these transcripts is affected by modifications at the wobble position of the tRNAs^{4,15}. Our work supports the idea that mRNAs encoding proteins involved in nutrient

Fig. 6 | Endosulfine, Gad8 and Elongator are required for efficient translation of certain mRNAs during quiescence entry. **a** Extracts from WT and *igo1Δ* cells expressing *gad8::L:HA*, were analysed by SDS-PAGE and immunoblotting with anti-HA antibodies during nitrogen starvation. Ponceau stain was used as a loading control. Immunoblot quantification was performed using Image Studio Lite software, $n = 2$. Data are presented as the mean \pm S.E.M. **b** Same as in (a), Gad8 phosphorylation state was analysed in WT and *igo1Δ* cell extracts. Immunoblot quantification was performed using Image Studio Lite software, $n = 2$. Data are presented as mean \pm S.E.M. **c** Same as in (a), *sgo2::L:HA* protein was analysed in a WT

and *gad8Δ* cell extracts. Immunoblot quantification was performed using Image Studio Lite software, $n = 2$. Data are presented as the mean \pm S.E.M. **d** Same as in (a), *sgo2::L:HA* protein was analysed in a WT and *elp3Δ* cell extracts. Immunoblot quantification was performed using Image Studio Lite software, $n = 2$. Data are presented as the mean \pm S.E.M. **e** Serial dilutions from cultures of WT, *igo1Δ*, *gsk3Δ* and *igo1Δ gsk3Δ* were spotted onto MMPhe (Minimal Media with Phenylalanine) plates without or with paromomycin (0.5 mg/ml). For gel source data, see Supplementary Fig. 9. Source data are provided as a Source data file.

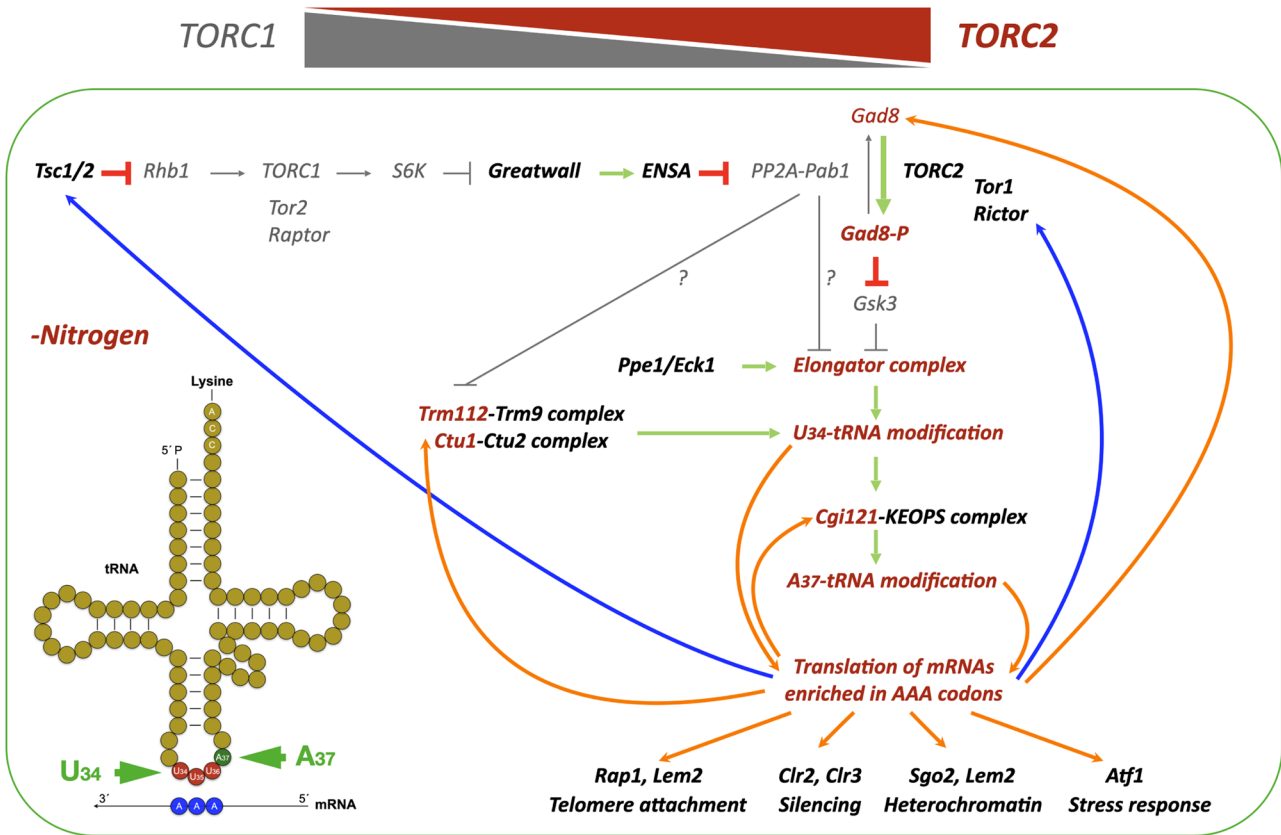


Fig. 7 | Activation of TORC2-Gad8 signalling in quiescent cells promotes the translation of mRNAs with a high AAA_{Lys} codon usage. This model is based on previous work in fission yeast, demonstrating that nitrogen starvation induces the inactivation of TORC1 and the activation of TORC2 signalling through the Greatwall-Endosulfine-PP2A/B55 pathway⁴⁻⁷. Phosphorylation of Gad8 at S546 leads to the inhibition of Gsk3 and the activation of Elongator, which promotes U₃₄ tRNA modification and translation of Tsc1, an inhibitor of TORC1, as well as activators of TORC2, such as Tor1 and Rictor (depicted by blue arrows)⁸. In this study, we present

additional feedback loops (indicated by orange arrows) that enhance the translation of Gad8, Trm112, Ctu1 and Cgi121, further increasing the U₃₄ and A₃₇ tRNA modifications necessary for the efficient translation of mRNAs enriched in AAA_{Lys} codons. Such mRNAs include *rap1*, *lem2*, *clr2*, *clr3* and *sgo2* which encode proteins required for the correct attachment of telomeres to the NE and for subtelomeric gene silencing, and *atf1*, which encodes the master regulator of the Core Environmental Stress Response (CESR) genes in fission yeast.

starvation, stress response or even the translation of viral RNA genomes present MoTTs, which are translated more efficiently under stress conditions^{8,12,13,67-70}. Related to this, Atf1, the master regulator of the Core Environmental Stress Response (CESR) genes in fission yeast, has been shown to be regulated by the Elongator and Trm9/Trm112 complexes. Atf1 translation and function are compromised in *elp3Δ*, *trm9Δ* or *trm112Δ* mutants upon oxidative stress^{12,13}. Atf1 protein levels are reduced in nitrogen-starved *igo1Δ* cells (Supplementary Fig. 8b), whereas *atf1* mRNA levels increase both in wild-type and *igo1Δ* cells (Supplementary Fig. 8c). Together, these results, suggest that the Greatwall-Endosulfine-PP2A/B55 pathway controls translation of *atf1* mRNA during nitrogen stress.

In animal cells, the Hif1 α mRNA is translated in drug-resistant melanomas through a mechanism involving the activation of Elp1 by the PI3 kinase signalling pathway. The activation of Hif1 α promotes

drug resistance by inducing anaerobic glycolysis⁷¹. Therefore, the mcm⁵s²U₃₄ modification in the tRNA anticodon promotes the translation of mRNAs enriched in AAA codons, including Hif1 α mRNA. This discovery opens new avenues for identifying inhibitors of Elongator and other tRNA modifiers to treat drug-resistant tumours and combat viral infections.

Methods

Strains and growth conditions

Yeast strains are listed in Supplementary Data 7. Fission yeast cells were cultured and genetically manipulated according to standard protocols⁷². Genetic crosses were performed on malt extract agar plates. Cells were typically cultured overnight at the appropriate temperatures in yeast extract supplemented with adenine, leucine, histidine, lysine, and uracil (YES), or in Edinburgh minimal medium

containing 93.5 mM ammonium chloride (EMM2) as a nitrogen source. For nitrogen starvation experiments, exponentially growing cells were shifted from Edinburgh minimal medium (EMM2) at 28 °C to minimal medium without nitrogen (EMM2-N) at 25 °C.

In overexpression experiments using the *nmf1*⁺ promoter, cells were grown to the logarithmic phase in EMM2 containing 15 μM thiamine. Then, the cells were harvested and inoculated in fresh EMM2 medium without thiamine.

DNA techniques and plasmid construction

Enzymes for molecular biology were obtained from Fermentas and Thermo Fisher. PCRs were performed with using Velocity DNA polymerase (Bioline). Oligonucleotides employed for strain and plasmid construction are listed in Supplementary Data 8. Information regarding construction strategies is available upon request. Plasmids used in this study carry the ampicillin resistance gene for selection in *E. coli* and are listed in Supplementary Data 8.

RNA Isolation, RNAseq and RT-qPCR

Wild type (2666), *igo1Δ* (2727) and *ppk18Δ cek1Δ* (2883) cells were grown to mid-exponential phase in EMM2, centrifuged and washed three times in EMM2-N, and cultured in EMM2-N at 25 °C. For RNAseq, 2×10^8 cells were harvested at times 0 and 4 h, washed with cold DEPC-H₂O, and snap frozen. RNA extraction was carried out by disrupting the cells with glass beads using RNAeasy Mini kit (Qiagen) and following the manufacturer's instructions. RNA quality was evaluated using the Bioanalyzer 2100 (Agilent). Library preparation, using the Illumina Ribo Zero and TruSeq Stranded kits, and subsequent NGS sequencing were performed by Macrogen. Sequencing quality was assessed with FastQC (v 0.11.8, Babraham Bioinformatics). If necessary, adaptors were trimmed using Trimmomatic (v 0.38)⁷³. Alignment was performed with HISAT2 v 2.1.0 (CCB in John Hopkins University)⁷⁴ using *S. pombe* reference genome from Pombase (downloaded on 30/11/2018). Samtools (v 1.9) and deepTools (v 3.3.0) were used to obtain bigWig files to visualize in IGV (v 2.4.16) and JBrowse (v 1.15.4) browsers. Read counts were obtained with featureCounts (Subread package v 1.6.3, Walter+Eliza Hall Bioinformatics)⁷⁵. DESeq2 (v1.22.2)⁷⁶ was used for the differential expression analysis. Plots representing upregulated genes in Endosulfine (*igo1Δ*) and Greatwall (*cek1Δ ppk18Δ*) mutants shown in Fig. 1a and Supplementary Fig. 1a were generated with karyoploteR (v 1.12.4)⁷⁷.

For RT-qPCR, total RNA was isolated from 2×10^8 *S. pombe* cells in exponential phase by disrupting the cells with glass beads in TRIzol[®] Reagent (Invitrogen) and following the manufacturer's instructions. The integrity of the RNA was verified through 1.2% agarose gel electrophoresis, and its quality and quantity were determined using a microspectrophotometer. RNA was treated with RNase-free DNase I (Invitrogen) at 25 °C for 30 min, following the manufacturer's instructions. Each RNA sample (1–2 μg) was then reverse transcribed with the SuperScript[™] First-Strand Synthesis System (Invitrogen) using the oligo(dT) primer supplied with the kit or the tRNA^{Lys}_{UUU} specific reverse primer in combination with the *act1* gene reverse primer (Supplementary Data 8) at 50 °C for 30 min in a 20 μl total volume. Quantitative PCR (qPCR) amplification of cDNA (1 μl) was carried out using TB Green Premix Ex Taq[™] (TaKaRa) and the primer pairs indicated in the Supplementary Data 8, in a 20 μl total volume with the following cycling parameters: 95 °C for 45 s, 40 cycles of 95 °C for 5 s and 60 °C for 31 s, followed by a dissociation step at 95 °C for 15 s, 60 °C for 1 min and 95 °C for 15 s. The reactions were run in duplicate or triplicate in an Applied Biosystems 7300 Real-Time PCR System. Negative controls without reverse transcriptase, without RT-primer and without cDNA were included to control for DNA contaminations. Fold changes in the expression levels relative to the wild-type strain grown in EMM2 were calculated according to the mathematic model described by ref. 78, with normalization to *act1* expression levels. The

experiments were performed at least twice with cDNA from different biological repeats.

SRFF microscopy

Samples were observed using a Confocal Andor Dragonfly 200 microscope, equipped with a 100x/1.45 Oil Plan Apo objective, an Andor sCMOS Sona 4.2B-11 camera and controlled by Fusion (SRRF-STREAM) software. ImageJ software was used for general image and movie manipulation. Radial Profile Analysis and the calculations of Pearson's Correlation Coefficients were performed using ImageJ. More than 100 nuclei were measured for each strain.

Staining knobs with DAPI

Exponentially growing and nitrogen-starved wild-type (JED142) and *igo1Δ* (JED187) fission yeast cells were stained with DAPI to visualize knobs following the protocol described by Matsuda et al., 2015²¹.

S. pombe protein extracts and western blot

TCA extraction was performed as previously described⁷⁹. For immunoblotting, PVDF membranes were probed with anti-HA (12CA5, Roche), anti-GFP (3H9, ChromoTek), anti-GST (RPN1236V, Cytiva), anti-P-Gad8 (kindly provided by José Cansado, University of Murcia, Spain) and anti-Atf1 antibodies^{12,80} (kindly provided by Elena Hidalgo, Pompeu Fabra University, Spain). Standard procedures were employed for protein transfer, blotting and chemiluminescence detection. Protein detection was performed using the ECL kit (BioRad). Uncropped and unprocessed versions gels and blots are shown in Supplementary Fig. 9.

Chromatin immunoprecipitation (ChIP)

Chromatin isolation and immunoprecipitation was performed as previously described⁸¹. *S. pombe* cell cultures were grown in EMM2 or after 4 hours of nitrogen starvation in EMM2-N to OD₆₀₀ of 0.5–0.6 and crosslinked with 1% formaldehyde for 10 min at room temperature. To terminate crosslinking, 2.5 M glycine was added to a final concentration of 125 mM for 5 min. Cells were pelleted by centrifugation, washed twice with 10 ml of cold PBS, frozen on dry ice and stored at –80 °C. Cell pellets from 50 ml cultures were resuspended in 0.25 ml of breaking buffer (0.1 M Tris-HCl pH 8.0, 20% glycerol, 1 mM PMSF) and lysed in a Fast-prep (2 cycles of 45 s) in the presence of glass beads (50 micron; Sigma) at 4 °C. Lysates were centrifuged at 14,000 g for 1 min at 4 °C. Pellets were washed with 1 ml of lysis buffer (50 mM HEPES pH 7.6, 140 mM NaCl, 1 mM EDTA, 1% Triton X-100, 0.1% sodium deoxycholate, 0.1% SDS, 1 mM PMSF). Pellets containing chromatin were resuspended in 0.25 ml of lysis buffer. Lysates were sonicated for 6 min at 4 °C (30 s on, 30 s off), using a water bath sonicator (Diagenode Bioruptor Plus), transferred to new 1.5 ml Eppendorf tubes, added 0.75 ml of lysis buffer and centrifuged at 14,000 g for 30 min at 4 °C. 50 μl of supernatant was kept as 'input' and the remainder (~950 μl) was subjected to immunoprecipitation with antibodies against K14-acetylated histone H3 (07-353, Upstate Biotechnology) and 20 μl of protein G agarose beads (100.04D, Dynabeads Protein G, Thermo Fisher). After an overnight incubation at 4 °C with mixing, beads were washed sequentially with 1 ml of lysis buffer once, lysis buffer + 500 mM NaCl twice, wash buffer (10 mM Tris pH 8.0, 1 mM EDTA, 250 mM LiCl, 0.5% sodium deoxycholate, 0.5% NP-40, 1 mM PMSF) twice, and TE buffer (10 mM Tris pH 7.5, 1 mM EDTA) once. Each wash was for 5 min with mixing at room temperature. Immune complexes were eluted in 100 μl elution buffer (50 mM Tris pH 8.0, 10 mM EDTA, 1% SDS) at 65 °C for 20 min. Beads were washed with 150 μl TE + 0.67% SDS, which was combined with the eluate. 150 μl TE + 0.67% SDS was also added to the input samples, and both IP and input samples were incubated at 65 °C overnight to reverse protein–DNA crosslinks. DNA was purified by phenol/chloroform extraction. Analysis by qPCR was carried out using a Bio-Rad CFX96 instrument, TB Green Premix Ex

Taq™ (TaKaRa), and primers listed in Supplementary Data 8. ChIP signals were calculated as IP/input and normalised to wild-type levels at $t = 0$ h with an assigned value of 1.

Immunoprecipitations and mass-spectrometry analysis

Immunoprecipitation was performed following previously established protocols⁵². For the immunoprecipitation of Paa1-L-YFP (strain JED62) and Pab1-L-YFP (strain JED56), 1 l of cells was grown to mid-log phase in EMM2, then shifted to EMM2-N for 1 h and crosslinked with 1% formaldehyde for 10 min at 25 °C. The reaction was quenched by adding glycine to 250 mM and incubating for 5 min on ice. Cells were collected by centrifugation, washed with PBS 1x, frozen in liquid nitrogen and broken with a Freezer/Mill in lysis buffer (25 mM Tris HCl pH 7.5, 150 mM NaCl, 0.5% SDS, 1% NP40, 1 mM PMSF, 1 µg/ml aprotinin, 1 µg/ml leupeptin, 1 µg/ml pepstatin). Cell lysates were then slowly diluted to 0.1% SDS final concentration for immunoprecipitation in lysis buffer without SDS at 4 °C for 30 min. Clarified extracts were immunoprecipitated by adding 40 µl of GFP-Trap beads (gta-20, Chromotek) for 1 h at 4 °C. The beads were washed six times with lysis buffer containing 500 mM NaCl. Finally, the beads were sent to the Proteomics Facility of the Salamanca Cancer Research Center for mass spectrometry analysis. Samples were tryptic digested in solution with sodium dodecyl sulfate (SDS) and desalted using solid-phase extraction disks for SDB-RPS StageTips. Reversed-phase LC-MS/MS analysis of peptides was performed using a nano-UHPLC system (NanoElute, Bruker Daltonics, Germany) coupled to a hybrid trapped ion mobility-quadrupole time-of-flight mass spectrometer Tims TOF Pro (Bruker Daltonics, Germany) via a modified nano-electrospray ion source (Captive Spray, Bruker Daltonics, Germany). Peptides were loaded onto a trapping column (Trap AcclaimPepMap 100 C18, Thermo) and were separated on a C18 1.9 µm 75ID 15cms Bruker fifteen at 40 °C using a 60 min gradient (from 2% to 35% ACN/0.1 FA). MS acquisition was run in data-dependent acquisition (DDA) mode (1.1) with PASEF. The acquired data were submitted to the MaxQuant (1.6.17.0) quantitative proteomics software package for identification and relative quantification by iBAQ. The UniProtKB database has been used using the revised sequences and isoforms from the *S. pombe* proteome (UP000002485 download 2021-11-29). Search parameters were as follows: fully tryptic digestion with up to two missed cleavages, 20 ppm and 40 ppm mass tolerances for precursor and product ions, respectively, oxidation of methionine and acetylation of the protein n-terminus were established as variable modifications and carbamidomethylation of cysteine as fixed modification. One percent false discovery rate (1% FDR) using Target-Decoy database for both peptide and protein validation was used. For protein identification one unique peptide was considered as the minimum number. Analysis and interpretation of the results were carried out using the String Database. Two experimental replicas of the mass spectrometry were performed. Extracts from the untagged wild-type strain were used as negative control in the immunoprecipitation experiment.

For the immunoprecipitation of GFP-Pab1 (strain 2895), 16 l of cells were grown to mid-log phase in EMM2 at 25 °C. After one day, half of the culture was shifted to EMM2-N for 1 h. Subsequently, cells were harvested by centrifugation and frozen at -80 °C. Cells were lysed using glass beads and a bead beater in 100 ml of NP-40 buffer (6 mM Na₂HPO₄, 4 mM NaH₂PO₄, 1% NP-40, 150 mM NaCl, 2 mM EDTA, 50 mM NaF and 0.1 mM Na₃VO₄) supplemented with complete EDTA-free protease inhibitor cocktail (Roche), 1.3 mM benzamidine (Sigma) and 1 mM PMSF (Sigma). Lysates were cleared by centrifugation, and supernatants were mixed with 60 µl of 50% slurry GFP-TRAP magnetic agarose beads (GFP-Trap® magnetic agarose, ChromoTek) equilibrated with NP-40 buffer. After 90 minutes of incubation at 4 °C, beads were magnetically separated from lysates and washed twice with 5 ml of NP-40 buffer. Samples were washed with 5 ml of low-NP-40 buffer (0.02% NP-40) to reduce total detergent in purified proteins and

subsequently resuspended in 1 ml of low-NP-40 buffer. Proteins were eluted twice with 150 µl of elution buffer (200 mM glycine-HCl pH 2.5) and precipitated for 30 minutes on ice using 100 µl of 100% TCA. Samples were then spun down for 30 minutes at 13000 rpm and 4 °C, washed with 1 ml of cold acetone containing 0.05 N HCl and 1 ml of cold acetone. Finally, pellets were dried at room temperature and stored at 4 °C for mass spectrometry analysis. A small amount of each sample was used to confirm proper purification of GFP-tagged proteins. For that purpose, the Plus One Silver Staining protein kit (GE Healthcare) was employed following manufacturer instructions. TCA-precipitated proteins were digested with trypsin and analyzed by two-dimensional liquid chromatography tandem MS (2D-LC-MS/MS) as previously described in ref. 83. MS2 and MS3 spectra were extracted separately from RAW files, and converted to DTA files using Scansifter software⁸⁴ (v2.1.25). Spectra with less than 20 peaks were excluded and the remaining spectra were searched using the SEQUEST algorithm (Thermo Fisher Scientific, San Jose, CA, USA; version 27, rev. 12). Sequest was set up to search the *S. pombe* protein database (pombe_contams_20151012_rev database, created in October 2015 from pombase.org). Common contaminants were added, and all sequences were reversed to estimate the false discovery rate (FDR), yielding 10390 total entries. Variable modifications (C + 57, M + 16, [STY] + 80 for all spectra and [STY]-18 for MS3), strict trypsin cleavage, <10 missed cleavages, fragment mass tolerance: 0.00 Da (because of rounding in SEQUEST, this results in 0.5 Da tolerance), and parent mass tolerance: 2.5 Da were allowed. Peptide identifications were assembled and filtered in Scaffold (v4.8.4, Proteome Software, Portland, OR) using the following criteria: minimum of 99% protein identification probability; minimum of two unique peptides; minimum of 95% peptide identification probability. FDRs were estimated in Scaffold based on the percentage of decoy sequences identified after using the above filtering criteria; the protein level FDR was 0.7% and the peptide level FDR was 0.3%. Proteins containing the same or similar peptides that could not be differentiated based on MS/MS alone were grouped to satisfy the principles of parsimony. Mass spectrometry identified proteins were exported from Scaffold to Excel for further analysis. Further analysis and interpretation of the results was carried out using the String Database (<https://string-db.org/>).

tRNA purification

tRNA purification assay was performed following established procedures⁸.

Quantification of tRNA modifications

The purified tRNAs (500 ng per sample) were subjected to hydrolysis in a 40 µl digestion cocktail containing 10 U of benzonase, 4 U of calf intestinal alkaline phosphatase, 0.12 U of phosphodiesterase I, 0.1 mM deferoxamine, 0.1 mM butylated hydroxytoluene, 4 ng pentostatin, 2.5 mM MgCl₂ and 5 mM Tris buffer (pH 8.0). The digestion mixture was incubated at 37 °C for 6 h. For the verification of HPLC retention times of RNA modifications, synthetic standards were employed. Analytical separation was facilitated by a Thermo Hypersil Gold aQ C18 column (100 × 2.1 mm, 1.9 µm), which was interfaced with an Agilent 1290 HPLC system and an Agilent 6495 triple quadrupole mass spectrometer. The employed LC system operated at 35 °C, maintaining a flow rate of 0.35 ml/min. The gradient starts with 100% solution A (0.1% formic acid in water) for 4 min, followed by a 4–15 min phase involving a transition from 0% to 20% solution B (0.1% formic acid in acetonitrile). The HPLC column was coupled with an Agilent 6495 triple quadrupole mass spectrometer, utilizing an electrospray ionization source in positive ion mode. Operational parameters were set as follows: gas temperature at 120 °C; gas flow rate at 11 l/min; nebulizer pressure at 20 psi; sheath gas temperature at 400 °C; sheath gas flow rate at 12 l/min; capillary voltage at 1500 V; and nozzle voltage maintained at 0 V. The dynamic multiple reaction monitoring mode was used for detection of

product ions derived from their respective precursor ions for all the RNA modifications. The collision energy was optimized to ensure maximal detection sensitivity for each modification. To ensure the same sample input, the MS signal intensity for each ribonucleoside was normalized with the UV signal intensity of canonical ribonucleosides. The fold change of the modified ribonucleosides in experiment group was calculated relative to the control group.

Drug sensitivity assays

For survival assays on agar plates, *S. pombe* strains were cultured in YES, diluted and the cells were spotted onto plates with minimal medium containing 93.5 mM NH₄Cl (EMM2) or 20 mM phenylalanine (MMPhe) without or with paromomycin (0.5 mg/ml), puromycin (0.5 mg/ml) or cycloheximide (2.5 µg/ml). The plates were then incubated at the indicated temperatures for 4–8 days.

Polysome fractionation

Polysome analysis was performed by sucrose gradient fractionation using the protocol described by Kressler et al. (1997)⁸⁵ with minor modifications. Wild-type (2666) and *igo1Δ* (2344) cells were grown to mid-exponential phase in EMM2, centrifuged and washed three times in EMM2-N, and cultured in EMM2-N at 25 °C for 4 h. 2×10^9 cells were harvested at times 0 and 4 h. Before harvest, cycloheximide was added at a final concentration of 150 µg/ml, and the cultures were placed immediately in ice water for 10 min. Cells were then collected by centrifugation at 3600 g for 5 min at 4 °C, washed with 20 ml of ice-cold breaking buffer (10 mM Tris-HCl pH 7.5, 100 mM NaCl, 30 mM MgCl₂ and 150 mg/ml cycloheximide), resuspended in 1 ml of breaking buffer, and pelleted by centrifugation at 14,000 g for 5 min at 4 °C. Cell pellets were immediately frozen in liquid nitrogen and broken with a Freezer/Mill in the presence of 0.5 ml of breaking buffer. Lysates were cleared by centrifugation at 14,000 g for 10 min at 4 °C.

Fifteen OD₂₆₀ units of supernatants were layered on 10 ml linear 10 to 50% sucrose gradients containing 50 mM Tris-acetate pH 7.5, 50 mM NH₄Cl, 12 mM MgCl₂, and 1 mM dithiothreitol, and centrifuged in an SW41 rotor at 4 °C at 39,000 rpm for 2 h 45 min. The gradients were scanned at 254 nm and fractionated in a Spectra/Chrom® Flow Thru UV monitor, taking 0.5 ml fractions. Two replicas of the experiment were performed and the polysome/monosome ratio (P/M ratio) was calculated. Total RNA from each fraction was isolated by adding 1 volume of TRIzol® Reagent (Invitrogen), according to the manufacturer's instructions with the following modifications. RNA was precipitated with isopropanol in the presence of 1/10 volume of 0.5 M sodium acetate pH 5.2, at –80 °C h for 1 h, and washed with 85% cold ethanol. Finally, RNA pellets were dissolved in 15 µl of DEPC-H₂O, combining RNA from two consecutive fractions. One-half of the RNA was resolved by electrophoresis on a 1.2% agarose gel, and the remaining half was used for cDNA synthesis as described above. cDNA was pooled into non-translating/poorly translating mRNA fractions (NT), corresponding to mRNAs associated with low molecular weight fractions, free ribosomal subunits and vacant ribosomes, and actively translating mRNAs found associated with the polysomal fractions (P). The mRNA levels (P/P + NT) for *rap1*, *ctu1*, *fil1* and *act1* were determined in the *igo1Δ* mutant relative to the wild type by qPCR, as described above.

Statistical methods

Average, S.E.M and *P* values for the two-way ANOVA were calculated using GraphPad Prism software. Data distribution was assumed to be normal, but this was not formally tested.

We used the normalized ratio at different time points as the dependent variable with different conditions (wild-type, *igo1Δ*, *igo1Δ P_{nmc41}:GST:pab1* + Thiamine or *igo1Δ P_{nmc41}:GST:pab1*-Thiamine in nitrogen-rich media or upon nitrogen starvation) treated as independent categorical variables, and sampling time as the covariate. We

modeled the NE/telomere overlay using ANCOVA as follow:

$$lm(\text{normalized ratio} \sim \text{time} * \text{label})$$

where time is the hours in nitrogen starvation, and label is the different conditions (wild-type, *igo1Δ*, *igo1Δ P_{nmc41}:GST:pab1* + Thiamine or *igo1Δ P_{nmc41}:GST:pab1*-Thiamine in nitrogen-rich media or upon nitrogen starvation).

Reporting summary

Further information on research design is available in the Nature Portfolio Reporting Summary linked to this article.

Data availability

The RNAseq data in this study has been deposited in NCBI's Gene Expression Omnibus under the accession numbers GEO Series accession number GSE217398 [<https://www.ncbi.nlm.nih.gov/geo/query/acc.cgi?acc=GSE217398>] and GSE269854. The mass spectrometry proteomics data has been deposited with the ProteomeXchange Consortium via the PRIDE partner repository, with the dataset identifiers PXD047703, PXD047697 and PXD047579. Further information and requests for reagents can be directed to the corresponding authors. Uncropped and unprocessed versions of images for gels and blots have been included as Supplementary Fig. 9. Source data are provided with this paper.

References

- Gonzalez, A. & Hall, M. N. Nutrient sensing and TOR signaling in yeast and mammals. *EMBO J.* **36**, 397–408 (2017).
- Gonzalez, A., Hall, M. N., Lin, S. C. & Hardie, D. G. AMPK and TOR: the Yin and Yang of cellular nutrient sensing and growth control. *Cell Metab.* **31**, 472–492 (2020).
- Bontron, S. et al. Yeast endosulfines control entry into quiescence and chronological life span by inhibiting protein phosphatase 2A. *Cell Rep.* **3**, 16–22 (2013).
- Chica, N. et al. Nutritional control of cell size by the Greatwall-Endosulfine-PP2A.B55 pathway. *Curr. Biol.* **26**, 319–330 (2016).
- Aono, S., Haruna, Y., Watanabe, Y. H., Mochida, S. & Takeda, K. The fission yeast Greatwall-Endosulfine pathway is required for proper quiescence/G(0) phase entry and maintenance. *Genes Cells* **24**, 172–186 (2019).
- Laboucarie, T. et al. TORC1 and TORC2 converge to regulate the SAGA co-activator in response to nutrient availability. *EMBO Rep.* **18**, 2197–2218 (2017).
- Martin, R. et al. A PP2A-B55-mediated crosstalk between TORC1 and TORC2 regulates the differentiation response in fission yeast. *Curr. Biol.* **27**, 175–188 (2017).
- Candiracci, J. et al. Reciprocal regulation of TORC signaling and tRNA modifications by Elongator enforces nutrient-dependent cell fate. *Sci. Adv.* **5**, eaav0184 (2019).
- Yarian, C. et al. Modified nucleoside dependent Watson-Crick and wobble codon binding by tRNALysUUU species. *Biochemistry* **39**, 13390–13395 (2000).
- Murphy, F. V. T., Ramakrishnan, V., Malkiewicz, A. & Agris, P. F. The role of modifications in codon discrimination by tRNA(Lys)UUU. *Nat. Struct. Mol. Biol.* **11**, 1186–1191 (2004).
- Kruger, M. K., Pedersen, S., Hagervall, T. G. & Sorensen, M. A. The modification of the wobble base of tRNAGlu modulates the translation rate of glutamic acid codons in vivo. *J. Mol. Biol.* **284**, 621–631 (1998).
- Garcia, P., Encinar Del Dedo, J., Ayte, J. & Hidalgo, E. Genome-wide Screening of Regulators of Catalase Expression: role of a transcription complex and histone and tRNA modification complexes on adaptation to stress. *J. Biol. Chem.* **291**, 790–799 (2016).

13. Fernandez-Vazquez, J. et al. Modification of tRNA(Lys) UUU by elongator is essential for efficient translation of stress mRNAs. *PLoS Genet* **9**, e1003647 (2013).
14. Endres, L., Dedon, P. C. & Begley, T. J. Codon-biased translation can be regulated by wobble-base tRNA modification systems during cellular stress responses. *RNA Biol.* **12**, 603–614 (2015).
15. Gu, C., Begley, T. J. & Dedon, P. C. tRNA modifications regulate translation during cellular stress. *FEBS Lett.* **588**, 4287–4296 (2014).
16. Hermand, D. Anticodon wobble uridine modification by Elongator at the crossroad of cell signaling, differentiation, and diseases. *Epigenomes* **4**, <https://doi.org/10.3390/epigenomes4020007> (2020).
17. Doi, A. et al. Chemical genomics approach to identify genes associated with sensitivity to rapamycin in the fission yeast *Schizosaccharomyces pombe*. *Genes Cells* **20**, 292–309 (2015).
18. Yadav, R. K., Matsuda, A., Lowe, B. R., Hiraoka, Y. & Partridge, J. F. Subtelomeric Chromatin in the Fission Yeast *S. pombe*. *Microorganisms* **9**, <https://doi.org/10.3390/microorganisms9091977> (2021).
19. Kanoh, J. Unexpected roles of a shugoshin protein at subtelomeres. *Genes Genet Syst.* **92**, 127–133 (2018).
20. Hirano, Y., Asakawa, H., Sakuno, T., Haraguchi, T. & Hiraoka, Y. Nuclear Envelope Proteins Modulating the Heterochromatin Formation and Functions in Fission Yeast. *Cells* **9**, <https://doi.org/10.3390/cells9081908> (2020).
21. Matsuda, A. et al. Highly condensed chromatins are formed adjacent to subtelomeric and decondensed silent chromatin in fission yeast. *Nat. Commun.* **6**, 7753 (2015).
22. Tashiro, S. et al. Shugoshin forms a specialized chromatin domain at subtelomeres that regulates transcription and replication timing. *Nat. Commun.* **7**, 10393 (2016).
23. Maestroni, L. et al. Nuclear envelope attachment of telomeres limits TERRA and telomeric rearrangements in quiescent fission yeast cells. *Nucleic Acids Res.* **48**, 3029–3041 (2020).
24. Chikashige, Y. et al. Membrane proteins Bqt3 and -4 anchor telomeres to the nuclear envelope to ensure chromosomal bouquet formation. *J. Cell Biol.* **187**, 413–427 (2009).
25. Inoue, H., Horiguchi, M., Ono, K. & Kanoh, J. Casein kinase 2 regulates telomere protein complex formation through Rap1 phosphorylation. *Nucleic Acids Res.* **47**, 6871–6884 (2019).
26. Fujita, I. et al. Telomere-nuclear envelope dissociation promoted by Rap1 phosphorylation ensures faithful chromosome segregation. *Curr. Biol.* **22**, 1932–1937 (2012).
27. van Emden, T. S. et al. Shelterin and subtelomeric DNA sequences control nucleosome maintenance and genome stability. *EMBO Rep.* **20**, <https://doi.org/10.15252/embr.201847181> (2019).
28. Kanoh, J., Sadaie, M., Urano, T. & Ishikawa, F. Telomere binding protein Taz1 establishes Swi6 heterochromatin independently of RNAi at telomeres. *Curr. Biol.* **15**, 1808–1819 (2005).
29. Harland, J. L., Chang, Y. T., Moser, B. A. & Nakamura, T. M. Tpz1-Ccq1 and Tpz1-Poz1 interactions within fission yeast shelterin modulate Ccq1 Thr93 phosphorylation and telomerase recruitment. *PLoS Genet* **10**, e1004708 (2014).
30. Hu, X., Liu, J., Jun, H. I., Kim, J. K. & Qiao, F. Multi-step coordination of telomerase recruitment in fission yeast through two coupled telomere-telomerase interfaces. *Elife* **5**, <https://doi.org/10.7554/eLife.15470> (2016).
31. Vazquez-Bolado, A. et al. The Greatwall-Endosulfine switch accelerates autophagic flux during the cell divisions leading to G1 arrest and entry into quiescence in fission yeast. *Int. J. Mol. Sci.* **24**, <https://doi.org/10.3390/ijms24010148> (2022).
32. Sugiyama, T. et al. SHREC, an effector complex for heterochromatic transcriptional silencing. *Cell* **128**, 491–504 (2007).
33. Job, G. et al. SHREC silences heterochromatin viadistinct remodeling and deacetylation modules. *Mol. Cell* **62**, 207–221 (2016).
34. Singh, N. S. et al. SIN-inhibitory phosphatase complex promotes Cdc11p dephosphorylation and propagates SIN asymmetry in fission yeast. *Curr. Biol.* **21**, 1968–1978 (2011).
35. Bourgeois, G., Letoquart, J., van Tran, N. & Graille, M. Trm112, a protein activator of methyltransferases modifying actors of the eukaryotic translational apparatus. *Biomolecules* **7**, <https://doi.org/10.3390/biom7010007> (2017).
36. Liger, D. et al. Mechanism of activation of methyltransferases involved in translation by the Trm112 ‘hub’ protein. *Nucleic Acids Res.* **39**, 6249–6259 (2011).
37. Agris, P. F., Vendeix, F. A. & Graham, W. D. tRNA’s wobble decoding of the genome: 40 years of modification. *J. Mol. Biol.* **366**, 1–13 (2007).
38. Karlsborn, T. et al. Elongator, a conserved complex required for wobble uridine modifications in eukaryotes. *RNA Biol.* **11**, 1519–1528 (2014).
39. Bauer, F. et al. Translational control of cell division by Elongator. *Cell Rep.* **1**, 424–433 (2012).
40. Huang, B., Johansson, M. J. & Bystrom, A. S. An early step in wobble uridine tRNA modification requires the Elongator complex. *RNA* **11**, 424–436 (2005).
41. Bjork, G. R., Huang, B., Persson, O. P. & Bystrom, A. S. A conserved modified wobble nucleoside (mcm5s2U) in lysyl-tRNA is required for viability in yeast. *RNA* **13**, 1245–1255 (2007).
42. Dewez, M. et al. The conserved wobble uridine tRNA thiolase Ctu1-Ctu2 is required to maintain genome integrity. *Proc. Natl. Acad. Sci. USA* **105**, 5459–5464 (2008).
43. Palmer, E., Wilhelm, J. M. & Sherman, F. Variation of phenotypic suppression due to the psi+ and psi- extrachromosomal determinants in yeast. *J. Mol. Biol.* **128**, 107–110 (1979).
44. Deutsch, C., El Yacoubi, B., de Crecy-Lagard, V. & Iwata-Reuyl, D. Biosynthesis of threonylcarbamoyl adenosine (t6A), a universal tRNA nucleoside. *J. Biol. Chem.* **287**, 13666–13673 (2012).
45. El Yacoubi, B. et al. A role for the universal Kae1/Qri7/YgjD (COG0533) family in tRNA modification. *EMBO J.* **30**, 882–893 (2011).
46. El Yacoubi, B. et al. The universal YrdC/Sua5 family is required for the formation of threonylcarbamoyladenine in tRNA. *Nucleic Acids Res.* **37**, 2894–2909 (2009).
47. Nedialkova, D. D. & Leidel, S. A. Optimization of codon translation rates via tRNA modifications maintains proteome integrity. *Cell* **161**, 1606–1618 (2015).
48. Su, C., Jin, M. & Zhang, W. Conservation and diversification of tRNA t(6)A-modifying enzymes across the three domains of life. *Int. J. Mol. Sci.* **23**, <https://doi.org/10.3390/ijms232113600> (2022).
49. Sarkar, S., Dalgaard, J. Z., Millar, J. B. & Arumugam, P. The Rim15-endosulfine-PP2A/Cdc55 signalling module regulates entry into gametogenesis and quiescence via distinct mechanisms in budding yeast. *PLoS Genet* **10**, e1004456 (2014).
50. Luo, X., Talarek, N. & De Virgilio, C. Initiation of the yeast G0 program requires Igo1 and Igo2, which antagonize activation of decapping of specific nutrient-regulated mRNAs. *RNA Biol.* **8**, 14–17 (2011).
51. Talarek, N. et al. Initiation of the TORC1-regulated G0 program requires Igo1/2, which license specific mRNAs to evade degradation via the 5′-3′ mRNA decay pathway. *Mol. Cell* **38**, 345–355 (2010).
52. Alvarez, B. & Moreno, S. Fission yeast Tor2 promotes cell growth and represses cell differentiation. *J. Cell Sci.* **119**, 4475–4485 (2006).
53. Hayashi, T. et al. Rapamycin sensitivity of the *Schizosaccharomyces pombe* tor2 mutant and organization of two highly phosphorylated TOR complexes by specific and common subunits. *Genes Cells* **12**, 1357–1370 (2007).

54. Ikai, N., Nakazawa, N., Hayashi, T. & Yanagida, M. The reverse, but coordinated, roles of Tor2 (TORC1) and Tor1 (TORC2) kinases for growth, cell cycle and separase-mediated mitosis in *Schizosaccharomyces pombe*. *Open Biol.* **1**, 110007 (2011).
55. Matsuo, T., Otsubo, Y., Urano, J., Tamanoi, F. & Yamamoto, M. Loss of the TOR kinase Tor2 mimics nitrogen starvation and activates the sexual development pathway in fission yeast. *Mol. Cell Biol.* **27**, 3154–3164 (2007).
56. Uritani, M. et al. Fission yeast Tor2 links nitrogen signals to cell proliferation and acts downstream of the Rheb GTPase. *Genes Cells* **11**, 1367–1379 (2006).
57. Weisman, R. & Choder, M. The fission yeast TOR homolog, tor1+, is required for the response to starvation and other stresses via a conserved serine. *J. Biol. Chem.* **276**, 7027–7032 (2001).
58. Weisman, R., Roitburg, I., Schonbrun, M., Harari, R. & Kupiec, M. Opposite effects of tor1 and tor2 on nitrogen starvation responses in fission yeast. *Genetics* **175**, 1153–1162 (2007).
59. Ebrahimi, H., Masuda, H., Jain, D. & Cooper, J. P. Distinct ‘safe zones’ at the nuclear envelope ensure robust replication of heterochromatic chromosome regions. *Elife* **7**, <https://doi.org/10.7554/eLife.32911> (2018).
60. Banday, S., Farooq, Z., Rashid, R., Abdullah, E. & Altaf, M. Role of inner nuclear membrane protein complex Lem2-Nur1 in heterochromatic gene silencing. *J. Biol. Chem.* **291**, 20021–20029 (2016).
61. Barrales, R. R., Forn, M., Georgescu, P. R., Sarkadi, Z. & Braun, S. Control of heterochromatin localization and silencing by the nuclear membrane protein Lem2. *Genes Dev.* **30**, 133–148 (2016).
62. Cohen, A. et al. TOR complex 2 in fission yeast is required for chromatin-mediated gene silencing and assembly of heterochromatic domains at subtelomeres. *J. Biol. Chem.* **293**, 8138–8150 (2018).
63. Atkins, J. F. & Bjork, G. R. A gripping tale of ribosomal frameshifting: extragenic suppressors of frameshift mutations spotlight P-site realignment. *Microbiol. Mol. Biol. Rev.* **73**, 178–210 (2009).
64. El Yacoubi, B., Bailly, M. & de Crécy-Lagard, V. Biosynthesis and function of posttranscriptional modifications of transfer RNAs. *Annu Rev. Genet.* **46**, 69–95 (2012).
65. Gustilo, E. M., Vendeix, F. A. & Agris, P. F. tRNA’s modifications bring order to gene expression. *Curr. Opin. Microbiol.* **11**, 134–140 (2008).
66. Jenner, L. B., Demeshkina, N., Yusupova, G. & Yusupov, M. Structural aspects of messenger RNA reading frame maintenance by the ribosome. *Nat. Struct. Mol. Biol.* **17**, 555–560 (2010).
67. Chan, C. T. et al. Reprogramming of tRNA modifications controls the oxidative stress response by codon-biased translation of proteins. *Nat. Commun.* **3**, 937 (2012).
68. Dedon, P. C. & Begley, T. J. A system of RNA modifications and biased codon use controls cellular stress response at the level of translation. *Chem. Res. Toxicol.* **27**, 330–337 (2014).
69. Jungfleisch, J. et al. CHIKV infection reprograms codon optimality to favor viral RNA translation by altering the tRNA epitranscriptome. *Nat. Commun.* **13**, 4725 (2022).
70. Patil, A. et al. Translational infidelity-induced protein stress results from a deficiency in Trm9-catalyzed tRNA modifications. *RNA Biol.* **9**, 990–1001 (2012).
71. Rapino, F. et al. Codon-specific translation reprogramming promotes resistance to targeted therapy. *Nature* **558**, 605–609 (2018).
72. Moreno, S., Klar, A. & Nurse, P. Molecular genetic analysis of fission yeast *Schizosaccharomyces pombe*. *Methods Enzymol.* **194**, 795–823 (1991).
73. Bolger, A. M., Lohse, M. & Usadel, B. Trimmomatic: a flexible trimmer for Illumina sequence data. *Bioinformatics* **30**, 2114–2120 (2014).
74. Kim, D., Langmead, B. & Salzberg, S. L. HISAT: a fast spliced aligner with low memory requirements. *Nat. Methods* **12**, 357–360 (2015).
75. Liao, Y., Smyth, G. K. & Shi, W. featureCounts: an efficient general purpose program for assigning sequence reads to genomic features. *Bioinformatics* **30**, 923–930 (2014).
76. Love, M. I., Huber, W. & Anders, S. Moderated estimation of fold change and dispersion for RNA-seq data with DESeq2. *Genome Biol.* **15**, 550 (2014).
77. Gel, B. & Serra, E. karyoploteR: an R/Bioconductor package to plot customizable genomes displaying arbitrary data. *Bioinformatics* **33**, 3088–3090 (2017).
78. Pfaffl, M. W. A new mathematical model for relative quantification in real-time RT-PCR. *Nucleic Acids Res.* **29**, e45 (2001).
79. Sanso, M., Gogol, M., Ayte, J., Seidel, C. & Hidalgo, E. Transcription factors Pcr1 and Atf1 have distinct roles in stress- and Sty1-dependent gene regulation. *Eukaryot. Cell* **7**, 826–835 (2008).
80. Garcia, P. et al. Binding of the transcription factor Atf1 to promoters serves as a barrier to phase nucleosome arrays and avoid cryptic transcription. *Nucleic Acids Res.* **42**, 10351–10359 (2014).
81. Sanso, M. et al. Cdk9 and H2Bub1 signal to Ctr6-Ctl1/Rpd3S to suppress aberrant antisense transcription. *Nucleic Acids Res.* **48**, 7154–7168 (2020).
82. Garcia, P. et al. Eng2, a new player involved in feedback loop regulation of Cdc42 activity in fission yeast. *Sci. Rep.* **11**, 17872 (2021).
83. Roberts-Galbraith, R. H., Chen, J. S., Wang, J. & Gould, K. L. The SH3 domains of two PCH family members cooperate in assembly of the *Schizosaccharomyces pombe* contractile ring. *J. Cell Biol.* **184**, 113–127 (2009).
84. Ma, Z. Q. et al. Supporting tool suite for production proteomics. *Bioinformatics* **27**, 3214–3215 (2011).
85. Kressler, D., de la Cruz, J., Rojo, M. & Linder, P. Fal1p is an essential DEAD-box protein involved in 40S-ribosomal-subunit biogenesis in *Saccharomyces cerevisiae*. *Mol. Cell Biol.* **17**, 7283–7294 (1997).
86. Kanoh, J. Telomeres and subtelomeres: new insights into the chromatin structures and functions of chromosome ends. *Genes Genet Syst.* **92**, 105 (2017).

Acknowledgements

We thank Rosa Degano and Nieves Ibarrola from the Salamanca Cancer Research Institute Proteomic Facility for their technical assistance in mass spectrometry analyses, Jorge Fernández-Vázquez, José Cansado, Yolanda Sánchez, Carlos R. Vázquez and Mercedes Tamame for sharing plasmids, antibodies and reagents, Jesús de la Cruz, Sara Martín, Rafael Daga, Silvia Salas and Ithaisa Medina for their help with the polysome analysis, and Pilar Pérez and members of the Moreno lab for their valuable discussions and comments on the manuscript. This work was funded by the Spanish Ministry of Science and Innovation-MCIN (grants BFU2017-88335-R and PID2020-115929RB-I00) and from the Castile and Leon government (grants CSI259P20, CSIO10P23 and IBSG Unit of Excellence programs CLU-2017-03 and CL-El-2021-08 co-funded by the P.O. Feder of Castile and Leon 14-20 and European Union ERDF “Europe drives our growth”) to S.M., and by the National Research Foundation of Singapore under its Singapore-MIT Alliance for Research and Technology Antimicrobial Resistance Interdisciplinary Research Group to J.S. and P.D.. The work in K.L.G.’s lab was supported by the National Institutes of Health R35GM131799, and in D.H.’s lab by PDR T.0012.14, CDR J.0066.16 and PDR T.0112.21 grants. D.H. is an honorary FNRS Director of Research and was affiliated with the University of Namur until November 23rd, 2023. N.G.-B. and A.V.-B. were funded by XFP15/03654, BES-2015-073171, predoctoral training contracts. R.L.-S.S. was funded by a predoctoral fellowship from the Castile and Leon government.

Author contributions

J.E.-D. led the project and conducted the experiments, excluding the RNAseq analysis performed by A.V.-B., the proteomic analyses conducted by R.L.-S.S. and J.-S.C. under the supervision of J.E.-D. and S.M., and K.L.G., respectively. The protein purifications used for MS analysis

and cell viability assay performed by N.G.-B. RNA purification, RT-qPCR analysis and polysome fractionation was carried out by M.B.S., ChIP assay was performed by P.G., tRNA purification was carried out by P.T. under the supervision of D.H. and tRNA modification analysis was conducted by J.S. under P.C.D.'s supervision. M.B.S., R.L.S.S. and A.V.-B. contributed equally to this work. J.E.-D., E.H., D.H. and S.M. discussed and interpreted the results. J.E.-D. and S.M. wrote the original draft. All authors contributed to editing the manuscript. S.M. supervised the work.

Competing interests

The authors declare no competing interests.

Additional information

Supplementary information The online version contains supplementary material available at <https://doi.org/10.1038/s41467-024-55004-4>.

Correspondence and requests for materials should be addressed to Javier Encinar del Dedo or Sergio Moreno.

Peer review information *Nature Communications* thanks the anonymous reviewers for their contribution to the peer review of this work. A peer review file is available.

Reprints and permissions information is available at <http://www.nature.com/reprints>

Publisher's note Springer Nature remains neutral with regard to jurisdictional claims in published maps and institutional affiliations.

Open Access This article is licensed under a Creative Commons Attribution-NonCommercial-NoDerivatives 4.0 International License, which permits any non-commercial use, sharing, distribution and reproduction in any medium or format, as long as you give appropriate credit to the original author(s) and the source, provide a link to the Creative Commons licence, and indicate if you modified the licensed material. You do not have permission under this licence to share adapted material derived from this article or parts of it. The images or other third party material in this article are included in the article's Creative Commons licence, unless indicated otherwise in a credit line to the material. If material is not included in the article's Creative Commons licence and your intended use is not permitted by statutory regulation or exceeds the permitted use, you will need to obtain permission directly from the copyright holder. To view a copy of this licence, visit <http://creativecommons.org/licenses/by-nc-nd/4.0/>.

© The Author(s) 2024